Sarcolemmal localisation of Na+/H+ exchange and Na+-HCO3- co-transport influences the spatial regulation of intracellular pH in rat ventricular myocytes.

.Carolina D. Garciarena, Yu-Ling Ma, Pawel Swietach, Richard D Vaughan-Jones, Laurence Huc

J Physiol 591.9 (2013) pp 2287–2306

The Journal of Physiology

Sarcolemmal localisation of Na^+/H^+ exchange and Na^+–HCO_3^- co-transport influences the spatial regulation of intracellular pH in rat ventricular myocytes

Carolina D. Garciarena, Yu-ling Ma, Pawel Swietach, Laurence Huc and Richard D. Vaughan-Jones

Burdon Sanderson Cardiac Science Centre, Department of Physiology, Anatomy and Genetics, Oxford OX1 3PT, UK

Key points

- Acid extrusion from ventricular myocytes typically occurs via Na^+/H^+ exchange (NHE1) and Na^+–HCO_3^- co-transporters (NBC). This maintains intracellular pH at ∼7.2: The membrane distribution of these transporters is uncertain.
- Immunofluorescence indicates that: NBC isoforms are located in lateral sarcolemma, intercalated discs and transverse tubules, whereas NHE1 is densely expressed at intercalated discs.
- Functional experiments with detubulated myocytes indicate reduced acid extrusion on NBC but no effect on NHE1 activity, confirming exclusion of NHE1 function from transverse tubules.
- Stimulating NHE1 activity induces sub-sarcolemmal $[H^+]_i$ depletion (forming local pH_i microdomains), particularly at intercalated discs, while stimulating NBC activity induces no pH_i microdomains.
- Our results provide the first demonstration that pH_i in ventricular myocytes is locally controlled through selective trafficking of membrane ion transporters. NHE1 preferentially controls pH_i at intercalated discs, where cell-to-cell gap-junctional channels are located, while NBC influences pH_i adjacent to transverse tubules, where key proteins for excitation–contraction coupling are located.

Abstract Membrane acid extrusion by Na^+/H^+ exchange (NHE1) and Na^+–HCO_3^- co-transport (NBC) is essential for maintaining a low cytoplasmic $[H^+]$ (∼60 nM, equivalent to an intracellular pH (pH_i) of 7.2). This protects myocardial function from the high chemical reactivity of H^+ ions, universal end-products of metabolism. We show here that, in rat ventricular myocytes, fluorescent antibodies map the NBC isoforms NBCe1 and NBCn1 to lateral sarcolemma, intercalated discs and transverse tubules (t-tubules), while NHE1 is absent from t-tubules. This unexpected difference matches functional measurements of pH_i regulation (using AM-loaded SNARF-1, a pH fluorophore). Thus, myocyte detubulation (by transient exposure to 1.5 M formamide) reduces global acid extrusion on NBC by 40%, without affecting NHE1. Similarly, confocal pH_i imaging reveals that NBC stimulation induces spatially uniform pH_i recovery from acidosis, whereas NHE1 stimulation induces pH_i non-uniformity during recovery (of ∼0.1 units, for 2–3 min), particularly at the ends of the cell where intercalated discs are commonly located, and where NHE1 immunostaining is prominent. Mathematical modelling shows that this induction of local pH_i microdomains is favoured by low cytoplasmic H^+ mobility and long H^+ diffusion distances, particularly to surface NHE1 transporters mediating high membrane flux. Our results provide the first evidence for a spatial localisation of $[H^+]_i$ regulation in ventricular myocytes,

DOI: 10.1113/jphysiol.2012.249664

suggesting that, by guarding pH_i, NHE1 preferentially protects gap junctional communication at intercalated discs, while NBC locally protects t-tubular excitation–contraction coupling.

(Received 7 December 2012; accepted after revision 13 February 2013; first published online 18 February 2013)
Corresponding author R. D. Vaughan-Jones: Burdon Sanderson Cardiac Science Centre, Department of Physiology, Anatomy and Genetics, Oxford OX1 3PT, UK. Email: richard.vaughan-jones@dpag.ox.ac.uk

Abbreviations AM, acetoxymethyl ester; Cx43, connexin 43; E–C coupling, excitation–contraction coupling; HDP, histidyl dipeptide; MCT, monocarboxylic acid transporter; NBC, Na^+–HCO_3^- co-transport; NCX, Na^+/Ca^{2+} exchange; NHE1, Na^+/H^+ exchange; ROI, region of interest; SERCA, sarcoplasmic reticulum Ca^{2+}-ATPase; tnC, troponin C; t-tubules, transverse tubules.

Introduction

Because of their high chemical reactivity, cytoplasmic H^+ ions are important modulators of cell function. Among their many effects in ventricular myocardium are a decrease in Ca^{2+} binding to troponin C (tnC) (Ball *et al.* 1994), changes of systolic and diastolic $[Ca^{2+}]$ (Choi *et al.* 2000; Saegusa *et al.* 2011), an inhibition of sarcolemmal Na^+/Ca^{2+} exchange (NCX) (Boyman *et al.* 2011) and sarcoplasmic reticulum Ca^{2+}-ATPase (SERCA) activity (Mandel *et al.* 1982) and, depending on conditions, either a stimulation or inhibition of sarcolemmal L-type Ca^{2+} current (Saegusa *et al.* 2011). These effects significantly influence cardiac contractility and excitability (for a recent review see Vaughan-Jones *et al.* 2009). H^+ ions are continuously generated as end-products of aerobic and anaerobic metabolism, a feature that is accentuated in heart by the physiological demand for rhythmic contraction. Excess H^+ ions must therefore be expelled (normal $[H^+]_i$ levels are ~60 nM, equivalent to an intracellular pH of ~7.2). Acid extrusion from ventricular myocytes relies on the co-ordinated activity of NHE (Na^+/H^+ exchange, isoform NHE1) and NBC (Na^+–HCO_3^- co-transport) (Lagadic-Gossmann *et al.* 1992; Leem *et al.* 1999). Electrogenic NBCe1 and electroneutral NBCn1 proteins have been identified in heart (Camilion de Hurtado *et al.* 1995; Damkier *et al.* 2006; De Giusti *et al.* 2011), although a recent report suggests a lack of NBCn1 in ventricular myocytes (Boedtkjer *et al.* 2008). Under conditions of high glycolytic flux, one or more monocarboxylic acid transporter (MCT) isoforms are also recruited to expel lactic acid (Halestrap *et al.* 1997). In clinical conditions such as myocardial ischaemia, when acid extrusion becomes insufficient to match intracellular acid production, the resulting fall of myocardial pH_i contributes to acute contractile failure and the appearance of electrical arrhythmia (Elliott *et al.* 1992; Orchard & Cingolani, 1994). Appropriate activity of the transporters is thus necessary for the maintenance of normal cardiac performance.

It has usually been assumed that pH_i regulatory transporters (pH-transporters) are expressed over the whole myocyte surface, including sarcolemma, transverse tubules (t-tubules) and intercalated discs. Indeed, immunofluorescence staining for NHE1 and NBCe1 proteins, the principal regulators of ventricular pH_i, has suggested various levels of expression in all three areas (Petrecca *et al.* 1999; Snabaitis *et al.* 2006; Lawrence *et al.* 2010; De Giusti *et al.* 2011). Many immunofluorescent probes, however, are poorly selective, and general membrane expression of pH-transporters in heart has yet to be confirmed. It is notable therefore that, in ventricular myocytes, many other types of ion transport protein display differential membrane expression. For example, L-type Ca^{2+} channels and NCX, key proteins involved in excitation–contraction coupling (E–C coupling), are mainly located in t-tubular membrane (Brette & Orchard, 2003), while gap-junctional channels, principally composed of connexin 43 (Cx43) protein, and responsible for anisotropic electric current flow in myocardium, are located at intercalated discs (Delmar & Sorgen, 2009), the specialised regions of cell-to-cell contact.

In the present work, we have determined the spatial location of NHE1 and NBC transport proteins in isolated mammalian ventricular myocytes, using a combination of protein immunofluorescence, real-time pH_i imaging and ultra-structural cell modification. By mapping the influence of NHE and NBC activity on local pH_i microdomains, and by comparing control cells with those where t-tubules have been physically removed through osmotic shock we have, for the first time, been able to correlate a spatially distributed pattern of immunofluorescence with a comparable distribution of functional pH-transporter activity. The results show that H^+ ion extrusion via NHE1 is excluded from certain surface membrane regions where intracellular acid is, instead, removed by HCO_3^- influx on NBC. Our results provide the first evidence for spatial localisation of pH_i regulation within the ventricular myocyte.

Methods

Ethical approval and myocyte isolation

All procedures involving animals have been approved by Oxford University ethics board in accordance with the Home Office (UK) Code of Practice and Animals (Scientific Procedures) Act 1986 guidelines. Ventricular myocytes were isolated from a total of 75 rats and 14

guinea-pigs. Briefly, 300 g adult male Sprague–Dawley rats or 400 g female adult guinea-pigs were killed by cervical dislocation. Isolated hearts were subjected to enzymatic digestion using either 0.077 mg ml^{-1} Liberase (Roche, Burgess Hill, UK) or a mixture of 0.4 mg ml^{-1} collagenase P (Roche, Burgess Hill, UK) and 0.04 mg ml^{-1} protease type XIV (Sigma-Aldrich, Poole, UK). For further details, see Lagadic-Gossmann *et al.* (1992). Ca^{2+}-tolerant, rod-shaped myocytes were selected for experiments.

Western blot and immunofluorescence

Ventricular myocytes were homogenised in lysis buffer. Denatured protein (40 μg) was subjected to 7% SDS-PAGE, transferred onto nitrocellulose membranes, blocked for 3 h with 5% non-fat milk and probed with appropriate primary antibodies (dilution 1:300 to 1:1000). Anti-mouse or anti-rabbit IgG conjugated to horseradish peroxidase (Dako, Ely, UK, 1:5000) were used as secondary antibodies. Detection was performed by ECL chemiluminescence kit (GE Healthcare, Little Chalfont, UK).

For immunostaining experiments, myocytes plated on poly-L-lysine-coated glass coverslips (Warner Instruments Inc., Hamden, CT, USA) were fixed with 4% paraformaldehyde in phosphate-buffered saline solution, permeabilised with 0.1% Triton X-100 and blocked with 1% bovine serum albumin. Myocytes were then incubated with 1:50 dilution of the primary antibody followed by incubation with 1:200 dilution of secondary antibodies coupled to Alexa Fluor 488 donkey anti-mouse or Alexa Fluor 647 donkey anti-rabbit (Invitrogen, Paisley, UK). In control experiments, samples were incubated with primary or secondary antibody alone. Coverslips were mounted on slides with fluorescent mounting medium (ProLong, Invitrogen, Paisley, UK). Images were acquired using an inverted laser scanning microscope (Leica SP5) equipped with a HCX PL APO ×40.0, 1.25 oil immersion objective lens. Excitation/emission wavelengths were 488 nm (argon laser)/500–600 nm and 633 nm (helium–neon laser)/> 650 nm, for Alexa Fluor 488 and Alexa Fluor 647, respectively. Pinhole was adjusted to 1.0 airy unit.

Primary antibodies: rabbit polyclonal anti-NBCe1, Millipore (Watford, UK); rabbit polyclonal anti-NBCn1 and -NBCe2, gifts from Dr J. Praetorius, Aarhus University; mouse monoclonal anti-NHE1, BD Biosciences (Oxford, UK); mouse monoclonal anti-L-type Ca^{2+} channel α2-subunit, Sigma-Aldrich (Poole, UK); and rabbit polyclonal anti-Cx43, Millipore (Watford, UK).

Detubulation

Detubulation was induced by rapid swelling of the cell following restoration of isotonic Tyrode solution, after a period of cell exposure to hypertonic conditions. This procedure causes t-tubules to detach from the surface membrane (Brette *et al.* 2002). Briefly, an aliquot of isolated rat ventricular myocytes was centrifuged at 130 *g* for 1 min and resuspended in 1 ml of Hepes-buffered Tyrode solution plus 1.5 M formamide. After 20 min, myocytes were centrifuged and the supernatant removed. Cells were then resuspended in 5 ml of Hepes-buffered Tyrode solution. Formamide-treated and control myocytes had the same morphological appearance; they could be electrically paced and loaded with fluorescent pH_i and Ca^{2+} indicators.

To assess the extent of detubulation, control and formamide-treated myocytes were incubated with the impermeant lipophilic fluorescent dye di-8-ANEPPS (10 μM, Invitrogen, Paisley, UK) for 10 min at room temperature, followed by 15 min washout. Fluorescence was confocally imaged using 488 nm excitation light with detection at >500 nm (Leica SP5). Settings were kept constant for both experimental groups.

Cell dimensions, length (l) and width (w), of cardiomyocytes were confocally determined. xy area was determined by two approaches: as the product lw (estimated area, considering rectangular shape) or as the surface outlined by the edges of the cell (measured area) using ImageJ (National Institutes of Health, Bethesda, MD, USA). Volume was calculated using $v = (\pi lwd)/4$, assuming the cell to be an elliptical cylinder, and the cell depth (d) was assumed to be 1/3 of the cell width (Boyett *et al.* 1991).

Electrophysiological techniques

Capacitance and L-type Ca^{2+} current were recorded in rat ventricular myocytes, using the whole-cell patch-clamp technique with 1–3 MΩ pipettes. Current signals were recorded using an Axopatch 200B amplifier and pCLAMP9 software (Axon Instruments, Union City, CA, USA).

Cell membrane capacitance. Cell membrane capacitance was measured by integrating the current recorded during a 10 mV depolarising pulse from the holding potential of −80 mV. Cell capacitance and series resistance were compensated by ∼70%. Pipette filling solution (in mM): KCl 130, Mg^{2+}-ATP 3, Na^+-GTP 0.4, EGTA 10, Hepes 25, pH 7.2 with KOH. Superfusion solution (in mM): NaCl 113, KCl 5, $MgSO_4$ 1, $CaCl_2$ 1, Na_2HPO_4 1, sodium acetate 20, glucose 10, Hepes 10, pH 7.4 with NaOH.

L-type Ca^{2+} current (I_{Ca}). From a holding potential of −80 mV, Ca^{2+} current was elicited by a test pulse to 0 mV, applied after a 100 ms prepulse to −40 mV to eliminate voltage-dependent Na^+ current. Intracellular Cs^+ was used to block K^+ currents. Pipette filling solution (in

mM): CsCl 12, NaCl 5, Hepes 10, Mg^{2+}-ATP 5, Na^+-GTP 1, phosphocreatine 5, TEACl 10, pH 7.1 with CsOH. Superfusion solution (in mM): NaCl 126, glucose 11, Hepes 24, $MgCl_2$ 1, $CaCl_2$ 1.08, CsCl 4.4, pH 7.4 with CsOH.

pH-transporter kinetics, pH_i and Ca_i^{2+} imaging

Myocyte superfusion solutions. Hepes-buffered Tyrode contained (in mM): Hepes 20, NaCl 135, KCl 4.5, $CaCl_2$ 1, $MgCl_2$ 1, glucose 11. NaCl was replaced osmotically by 5, 10, 20 or 30 mM NH_4Cl for ammonium-containing solutions; and by *N*-methyl-D-glucamine for Na^+-free solutions. pH was adjusted to 7.4 with 4 M NaOH or 5 M HCl at 37°C.

CO_2/HCO_3^--buffered Tyrode solution contained (in mM): $NaHCO_3$ 22, NaCl 125, KCl 4.5, $CaCl_2$ 1, $MgCl_2$ 1, glucose 11. $NaHCO_3$ was omitted and KCl was replaced osmotically by $KHCO_3$ for Na^+-free CO_2/HCO_3^- solutions. KCl (45 mM) was used for high K^+ solutions and NaCl concentration was reduced accordingly. pH was adjusted to 7.4 by bubbling with 5% CO_2–95% air at 37°C for at least one hour prior to starting experiments.

Whole-cell pH_i epifluorescence. Whole-cell pH_i was measured by epifluorescence in superfused, isolated myocytes, loaded with the acetoxymethyl ester (AM) form of SNARF-1 (carboxy-seminaphthorhodafluor-1), a fluorescent pH indicator (10 μM, Molecular Probes, Paisley, UK). The intracellular dye was excited by light (540 nm) from a 100 W xenon lamp. Emission at 590 and 640 nm was measured by two photomultiplier tubes, digitised by an analog–digital converter (MiniDigi 1A, Axon Instruments), and filtered at 10 Hz. The intracellular SNARF-1 ratiometric signal was calibrated in pH units *in situ* using the nigericin technique (10 μM nigericin, 140 mM KCl superfusates adjusted to pH 5.0, 5.5, 6.0, 6.5, 7.0, 7.5, 8.0, e.g. Leem *et al.* 1999).

Estimating flux activity for NHE1 and NBC. H^+ efflux (J_H) was estimated from whole-cell pH_i recovery rate (dpH_i/dt), following an acid load induced by the NH_4Cl prepulse technique, as $J_H = \beta_{tot} \times dpH_i/dt$, where β_{tot} is total intracellular buffering capacity. β_{tot} was calculated as the sum of intracellular buffering due to CO_2/HCO_3^- (β_{CO_2}) and the intrinsic (non-CO_2) buffering capacity (β_{int}). β_{int} was estimated from pH_i changes induced by stepwise removal of extracellular NH_4Cl (30 mM, 15 mM, 5 mM, 0 mM) in the presence of 30 μM cariporide (Sanofi-Aventis) to inhibit NHE1 activity, as described previously (Zaniboni *et al.* 2003). CO_2-dependent buffering was calculated as $\beta_{CO_2} = 2.3[HCO_3^-]_i$ where $[HCO_3^-]_i$ was calculated from the Henderson-Hasselbalch equation for given values of pH_i and P_{CO_2}, assuming full equilibration of the extrinsic buffer, as previously described (Leem *et al.* 1999). β_{CO_2} was assumed to be zero when Hepes-buffered solutions were used.

Confocal spatial imaging of pH_i. To analyse pH_i non-uniformity, cells were imaged confocally (Leica SP5, HCX PL APO ×40.0, 1.25 oil immersion objective) during the recovery from an acid load induced by NH_4Cl prepulse (NH_4Cl concentration: 30, 20, 10 or 5 mM). SNARF-1 was excited (514 nm argon laser), and fluorescence emission simultaneously collected by two photomultiplier tubes at 630–650 and 580–600 nm, respectively. Pinhole size was set at 1.0 airy unit. Images in *xyt* mode were acquired at 512 × 512 pixels every 0.753 s. ImageJ (National Institutes of Health, Bethesda, MD, USA) was used to convert the fluorescence images to 8-bit grey-scale stacks (which were background subtracted, ratioed and converted to pH units). To perform the spatial analysis, longitudinal pH_i gradients were defined as the average pH_i imaged in ROIs (regions of interest) at both ends of the cell (sub-sarcolemmal regions) minus average pH_i in an ROI at the centre of the cell. The ROIs covered the width of the cell (w) and their length was $l/20$ for end regions (where l is whole-cell length), and $6l/20$ in the centre region (see schematic diagram in Fig. 4*Da*). An in-house macro ensured that the external boundary of an ROI was coincident with the sarcolemmal outline of the cell. Radial pH_i gradients were calculated as the pH_i difference between sub-sarcolemmal ROIs spanning the length of the cell (of width $w/20$) and a central region of comparable length, and a width of $6w/20$ (schematic diagram in Fig. 4*Db*). Concentric pH_i gradients were calculated as the pH difference between a sub-sarcolemmal ROI, drawn to be coincident with the sarcolemmal outline of the cell (width = $w/20$ along the major, and $l/20$ along the minor axes) and a central ROI of dimensions $(6w/20) \times (6l/20)$ (schematic diagram in Fig. 4*Dc*).

Confocal spatial imaging of Ca_i^{2+}. Cells, loaded with the AM form of the Ca^{2+}-sensitive fluorescent indicator Fluo-3 (10 μM, Molecular Probes, Paisley, UK), were superfused with Hepes-buffered Tyrode solution and stimulated at 2 Hz by extracellular platinum electrodes. Fluo-3 was excited at 488 nm and emitted fluorescence collected at >505 nm. Line scans were recorded at 5 ms intervals over the width of the cell. After subtracting background fluorescence, the Fluo-3 time course signal was presented as a ratio of fluorescence/baseline fluorescence (F/F_o).

All chemicals were analytical reagent quality from Sigma-Aldrich (Poole, UK), except where otherwise specified.

Statistics

Data are presented as mean ± SEM. Student's unpaired *t* test was used, except where indicated, to compare data between experimental groups; $P < 0.05$ was considered significant.

Results

Immunofluorescence

Immunofluorescence for NHE1, NBCe1 and NBCn1 was measured with antibodies raised against cytoplasmic domains of the transporters. Their specificity was first examined by Western blot of rat ventricular myocyte protein homogenates (Fig. 1*A*). Polyclonal NBCe1 antibody (Millipore) showed a major band at approximately 120 kDa and a minor band at ∼85 kDa, similar to that found in rat kidney (Schmitt *et al.* 1999). For NBCn1, an affinity-purified antibody raised against the N-terminus of the electroneutral NBC produced a single band of a similar molecular weight to that previously published for left ventricle homogenates (Damkier *et al.* 2006). For NHE1, a monoclonal antibody raised against amino acids 682–801 of rat NHE1 recognised a major band at ∼100 kDa, in agreement with a previous report (Snabaitis *et al.* 2006).

To explore the spatial distribution of pH-transporters, fixed and permeabilised rat myocytes were incubated with the antibodies coupled to anti-rabbit or anti-mouse Alexa Fluor 488 and confocally imaged ($n = 4$–60). Results are shown in Fig. 1*B*. Immunostaining for both NBCe1 and NBCn1 appeared in the lateral sarcolemma and intercalated discs, accompanied by a strong transverse striated pattern, suggestive of trafficking to the t-tubules. In contrast, immunostaining for NHE1 was present in lateral sarcolemma, very prominent at intercalated discs, and exhibited a more punctate and fainter distribution within the intracellular compartment. No labelling was detected in control experiments in which primary or secondary antibodies were omitted (not shown).

Expression of NBCe2, a second electrogenic NBC isoform was also explored, as transcripts have been reported in human heart (Pushkin *et al.* 2000). The primary antibody, again raised against a cytoplasmic epitope, recognised protein of appropriate molecular weight by Western blot in ventricular myocyte homogenates (Supplemental Fig. S1, available online only). Multiple additional bands, however, were evident (28–230 kDa), suggesting lack of antibody specificity. Immunofluorescence also revealed general non-selective staining throughout the intracellular compartment. Clear evidence for membrane expression of NBCe2 was thus lacking.

Protein colocalisation experiments were performed on isolated ventricular myocytes, using an antibody against L-type Ca^{2+} channels, whose expression is highest in t-tubules; (Brette *et al.* 2006), or against Cx43 protein, which is highly expressed at intercalated discs (Delmar & Sorgen, 2009). Figure 1*C* top panel shows that L-type Ca^{2+} channels (red) and NBCe1 (green) immunofluorescence appeared in an overlapping striated array, coloured orange in merged images, consistent with common trafficking to t-tubules. This was confirmed in normalised longitudinal line-scans (to right of panel *C*) which displayed oscillatory patterns for L-type Ca^{2+} channels and NBCe1 immunofluorescence, with an in-phase periodicity of ∼1.5 μm (fixed myocytes). NBCe1 protein thus colocalises with L-type Ca^{2+} channels in the t-tubules. Figure 1*C* lower panel shows the results of dual labelling with antibodies against NHE1 (red) and Cx43 (green). In this case, staining for both proteins was highly localised at the intercalated disc regions of the cell, as also shown in the longitudinal line scan (to right of panel *C*), with no significant colocalisation elsewhere.

In myocytes dual-labelled with antibodies against NHE1 (red) and NBCe1 (green), colocalisation was not evident in t-tubules, either from merged 2-D images (Fig. 1*D*) or in longitudinal or radial line scans (to right of panel *D*). In the line scans, while NHE1 fluorescence within the cell compartment showed some oscillatory patterning, it was more irregular and not consistently in phase with that for NBCe1 (see amplified panels to the right of the longitudinal and radial scans). Clear colocalisation was, however, evident in surface sarcolemma and at the intercalated discs (see line scans and magnified fluorescence images at the bottom of panel *D*).

In summary, immunostaining suggests that NBCe1 and NBCn1 are expressed in all three membrane regions: lateral sarcolemma, intercalated disc and t-tubules. In contrast, NHE1 is largely excluded from t-tubules and, although expressed in both sarcolemma and intercalated discs, it is most prominent in the latter. NBC protein is thus generally expressed at surface membrane sites, while NHE1 expression appears more restricted.

Detubulation

The immunohistochemical work described above provides evidence for pH-transporter location, but cannot confirm functional activity. One way of evaluating this was to use intracellular SNARF-1 fluorescence to compare the kinetics of pH_i regulation in isolated rat ventricular myocytes, with and without t-tubules.

Detubulation was achieved by transient exposure of cells to hypertonic shock (Brette *et al.* 2002), i.e. suspending cells for 20 min in 1.5 M formamide, followed by a return to normal Tyrode solution; see Methods for details. The success of the detubulation procedure was

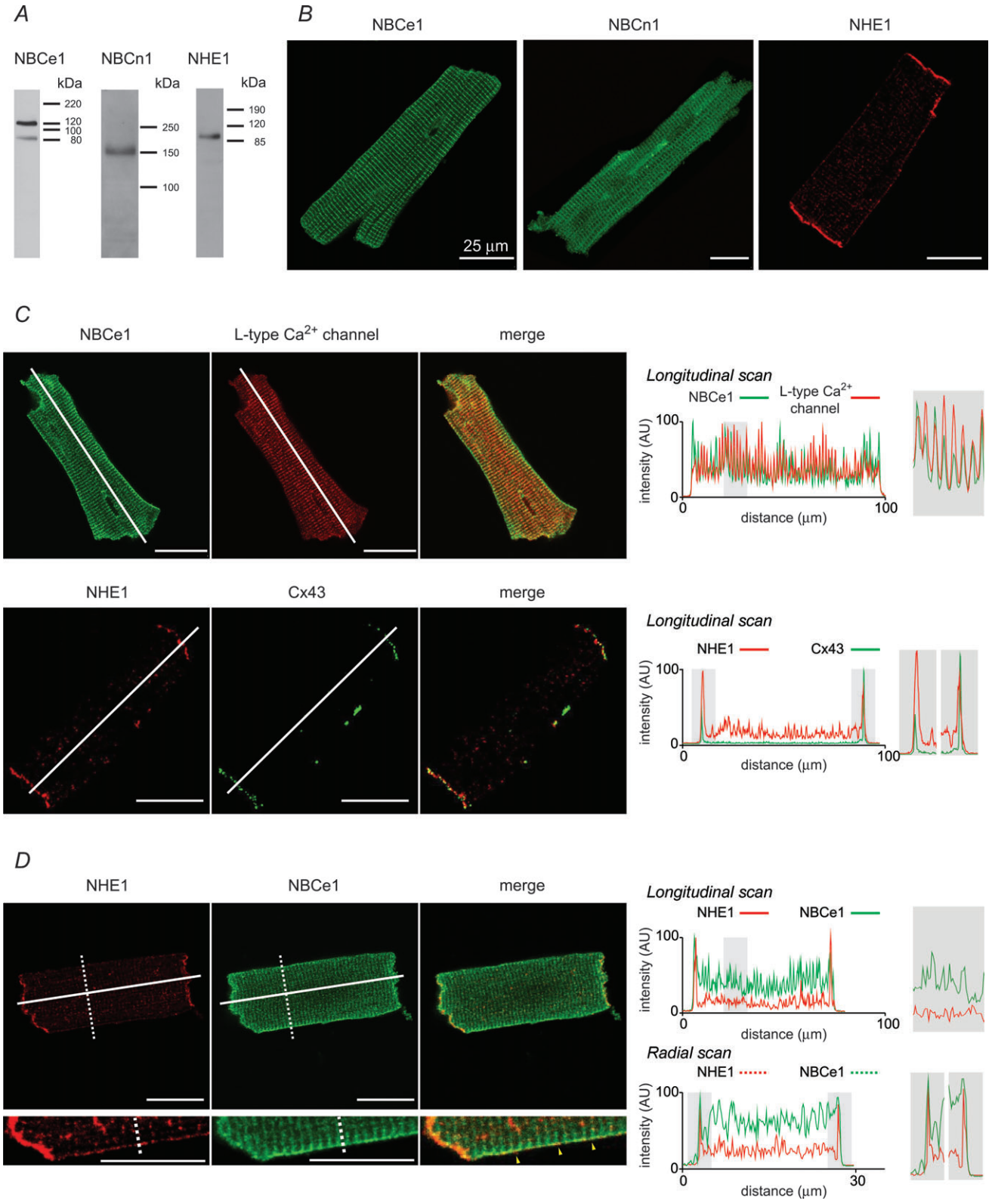

Figure 1. Immunofluorescence localisation of NHE1 and NBC
A, typical Western blots on protein samples of rat ventricular cardiomyocyte homogenates showing the specificity of antibodies used. *B*, confocal images of rat ventricular myocytes stained with the appropriate primary antibodies against the pH-transporters and Alexa Fluor-coupled secondary antibodies. NBCe1 and NBCn1, green; NHE1, red. Images are representative of 4–60 cells from at least 4 hearts. Scale bar: 25 μm. *C*, colocalisation experiments to

assessed by imaging the surface membrane of intact cells with the membrane-impermeant, fluorescent dye, di-8-ANEPPS, as shown in Fig. 2*A* (note the absence of major surface membrane invaginations in detubulated cells). Detubulation was also assessed (i) by electrophysiological measurement of whole-cell membrane capacitance, which was reduced by 40–60% (Fig. 2*B*), in agreement with previous work (Despa *et al.* 2003), (ii) by whole-cell voltage-clamp measurement of peak L-type Ca^{2+} current density (I_{Ca}), which was reduced by ∼50% (Fig. 2*C*), and (iii) by confocally imaging the electrically evoked Ca^{2+} transient (Fluo-3), which revealed a slower Ca^{2+} rise in intracellular core *versus* peripheral zones after detubulation (Fig. 2*D*; cf. Brette *et al.* 2002).

Detubulation appeared not to affect a ventricular myocyte's outline dimensions, suggesting that cell volume was not altered (Fig. 2*E*; for further details of volume measurement, see Methods and Supplemental Fig. S2). The cell's intrinsic intracellular H^+ buffering capacity, β_{int}, was also unaffected (Fig. 2*F*; β_{int} estimated from the stepwise pH_i decrease associated with a serial reduction in extracellular NH_4Cl concentration; see e.g. Leem *et al.* 1999). The effect of ventricular myocyte detubulation on pH_i regulation could then readily be compared by quantifying acid extrusion ($\beta_{int} \times dpH_i/dt$) from the pH_i recovery following an acute intracellular acid load (induced by 20 mM ammonium prepulse).

For myocytes superfused with CO_2/HCO_3^--free Tyrode solution (i.e. Hepes-buffered), pH_i recovery is mediated exclusively via NHE1 activity (Leem *et al.* 1999). The rate of this recovery was the same in normal and detubulated cells (Fig. 3*A*, top panel). In contrast, when myocytes are superfused with CO_2/HCO_3^--buffered Tyrode in the presence of the NHE1 inhibitor cariporide (30 μM), NBC isoforms are the sole means for acid extrusion (Lagadic-Gossmann *et al.* 1992; Leem *et al.* 1999). Under these conditions, the rate of pH_i recovery was much slower in detubulated cells (Fig. 3*B*, top panel). Results from several cells have been averaged in the graphs shown in Fig. 3*A* and *B*, which plot acid efflux on NHE1 and generic NBC (i.e. the combined effect of NBCe1 and NBCn1) *versus* pH_i. Over the pH_i range tested, efflux on NHE1 was unaffected by detubulation, while that through NBC was reduced by up to 43%. These results indicate that t-tubules harbour a significant fraction of the cell's NBC activity but none of its NHE1 activity. This finding is in good agreement with the spatial distribution of NHE1 and NBC proteins obtained above from immunofluorescence, which indicates minimal NHE1 expression in t-tubules.

Spatial pH_i non-uniformity

The location of pH-transporters at different membrane sites has important implications for the spatial control of pH_i. There will be considerable diffusion distances for H^+ ions to membrane transporters if the latter are excluded from t-tubules. For example, the distance from the centre of a myocyte to an intercalated disc region may be as much as 50 μm (typical ventricular cell length is 100 μm), while the radial distance may be 14 μm (Supplemental Fig. S2). Given the low mobility for intracellular H^+ ions (∼120-fold lower than in pure water, caused by fixed intracellular buffers) (Zaniboni *et al.* 2003), membrane acid extrusion might be expected to generate spatial pH_i gradients over these relatively long cytoplasmic distances. In contrast, significant transporter expression in t-tubular membrane would reduce local H^+ diffusion distances to 2 μm or less, given that tubular invagination occurs at sarcomere boundaries, which could minimise cytoplasmic gradient formation in these regions. Cytoplasmic gradients of 0.1–0.2 pH units have previously been observed (Swietach & Vaughan-Jones, 2005*b*; Vaughan-Jones *et al.* 2009). We therefore confocally imaged pH_i in isolated rat ventricular myocytes during selective stimulation of NHE1, generic NBC, or both, in order to discern the effect on pH_i.

Effect of NHE1 stimulation. Figure 4*A* illustrates schematically the experimental protocol. Ammonium prepulses (5–30 mM) were used to induce intracellular acid loads of differing magnitude, while superfusing the cell with Na^+-free solution to inhibit NHE1 and NBC activity. Under these conditions, pH_i appeared spatially uniform. Re-addition of Na^+_o to the superfusate activated NHE1 (NBC activity is negligible when solutions are CO_2/HCO_3^--free, buffered with Hepes) at

test NHE1 and NBC localisation against membrane proteins of known spatial distribution. Top: NBCe1 (green), L-type Ca^{2+} channel (red). Bottom: NHE1 (red), Cx43 (green). In the merged images, orange colour shows where green and red fluorescence signals colocalise spatially. Fluorescence intensity profiles were normalised to the peak (arbitrary units, AU) along the longitudinal white line depicted in the images. A fraction of each graph has been expanded on the right, to illustrate the presence or absence of overlapping fluorescence profiles. *D*, colocalisation experiments for NHE1 (red), NBCe1 (green). Longitudinal and transverse line scans were obtained from the raw images and fluorescence intensity was normalised to the respective line scan peak. These line scans, and the magnified images in the bottom panels, show colocalisation of NHE1 with NBCe1 at intercalated discs and the lateral sarcolemma (indicated by yellow arrows). Control experiments using primary or secondary antibody alone produced no fluorescence signal (data not shown).

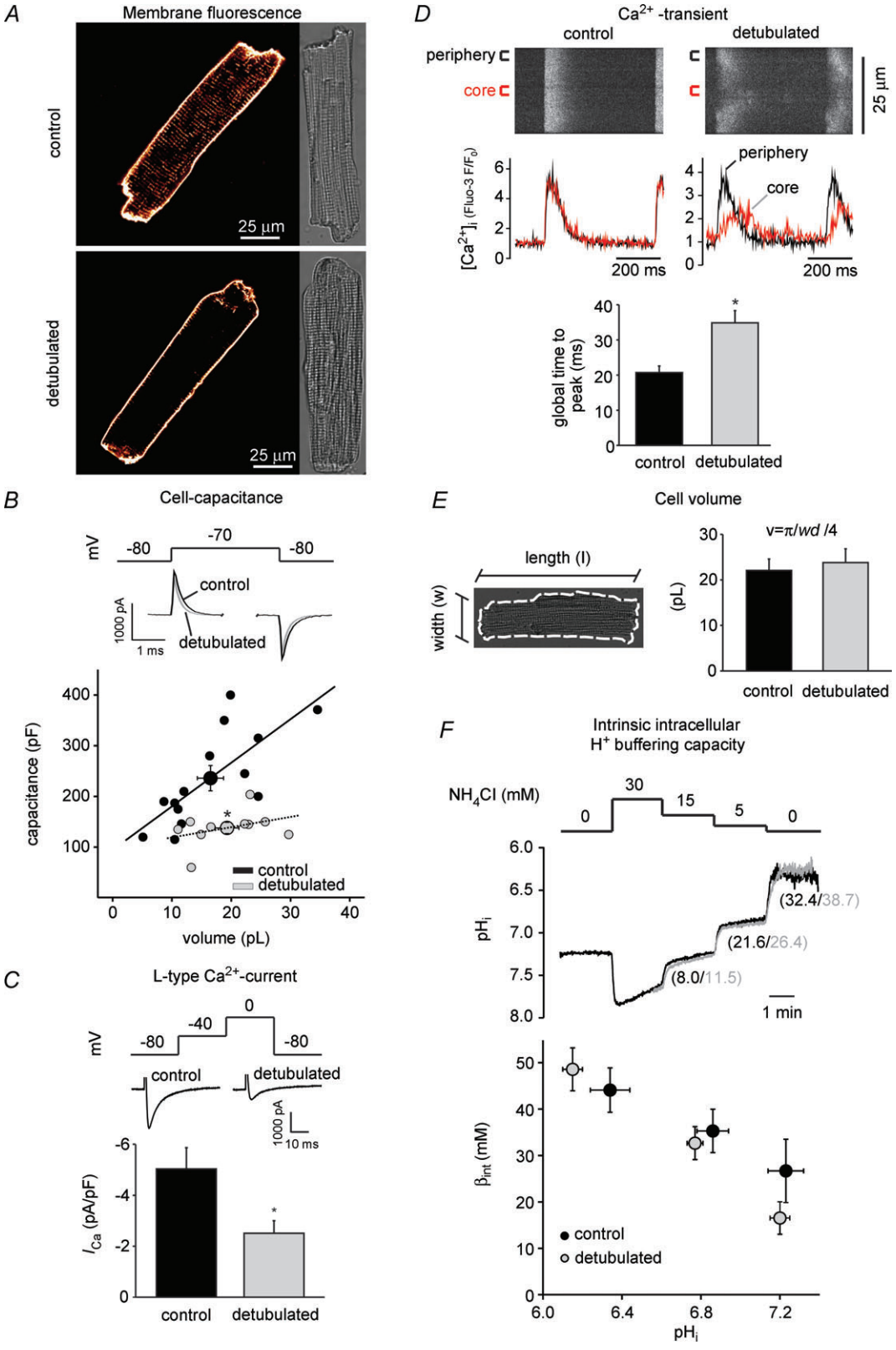

a rate determined by the level of acid loading. Figure 4*B* illustrates that, upon reactivating NHE1 from a pH_i of 6.25, the end-regions of the myocyte alkalinise more promptly and at a faster rate than a selected central region (the positioning of the regions of interest (ROIs) used for the pH measurements is shown in the cell image in Fig. 4*B*). The result suggests that a greater component of H^+ extrusion occurs from the ends of the cell.

The time delay for pH_i changes between end and central regions was up to 4 s (the time delay can be better appreciated in the inset to Fig. 4*B*). As a result, global pH_i recovery in the myocyte was associated with the appearance of a $[H^+]_i$ gradient, arranged longitudinally from the central region to each end of the cell. This is illustrated in Fig. 4*C*, where the size of the gradient (expressed in pH units, i.e. end-pH_i minus central-pH_i) has been plotted *versus* time, for the whole recovery period. The pH_i gradient rose from a starting value close to zero (i.e. a spatially uniform pH_i) to a peak of 0.09 pH_i units, 30 s after NHE1 reactivation, with end regions being consistently more alkaline than the central region. The gradient then declined over the following 2 min, such that pH_i non-uniformity had disappeared once the recovery was complete, and NHE1 activity had returned to its control level. Transient NHE1 stimulation by acute acidosis is thus able to induce significant and relatively longstanding pH_i non-uniformity ($>$2 min).

Figure 4*Da* shows a family of superimposed longitudinal pH_i gradient time courses, obtained when NHE1 was reactivated from different levels of acid loading. The peak size of the gradient was dependent on the level of NHE1 activity, being smaller when the starting pH_i had been prepulsed to a less acid level. Thus the gradients are related not only to the possible geometrical positioning of the transporters, but also to the membrane H^+ efflux density that they produce. This was confirmed by plotting (Fig. 4*E*; filled circles) peak size of the longitudinal pH_i gradient *versus* global NHE1-mediated H^+ efflux (estimated as whole-cell $\beta_{int} \times dpH_i/dt$; see Methods). The relationship is linear, indicating that a higher membrane H^+ efflux more readily raises local pH_i in end relative to central regions.

NHE1 stimulation also generated *radial* pH_i gradients. After readdition of Na^+_o, sub-membranous pH_i in lateral sarcolemmal regions recovered from an acid load faster than in a core region, positioned one radial distance ($\sim$14 μm) away, resulting in a radial gradient of up to 0.05 pH units. This is illustrated by the family of gradient time courses superimposed in Fig. 4*Db* (a radial gradient was measured as (submembranous pH_i – core pH_i), see inset to Fig. 4*Db*). This is the first time such radial gradients have been resolved in a ventricular myocyte, suggesting a functional expression of NHE1 at the lateral sarcolemma as well as at the ends of the cell. Peak radial gradients, however, were smaller than the longitudinal gradients, but were still graded according to the magnitude of global acid efflux. This is confirmed in the graphical plot shown in Fig. 4*E* (open circles), which shows that radial pH_i gradients increase linearly with NHE1 flux activity, but with a slope roughly 50% of that for longitudinal gradients. As a final check for pH_i non-uniformity, Fig. 4*Dc* shows time courses for pH_i gradients detected after NHE1 reactivation, but measured between the whole sub-membranous compartment and a central core region (irrespective of longitudinal or radial orientation; see inset to Fig. 4*Dc*). Once again, a transient spatial pH_i gradient was evident during NHE1 stimulation, with a peak of 0.08 pH_i units at high NHE1

Figure 2. Detubulation of rat ventricular myocytes
Formamide-induced osmotic shock physically and functionally uncouples t-tubules from the surface membrane. *A*, representative confocal images of cardiomyocytes stained with 10 μM di-8-ANEPPS, an impermeant membrane dye. Top: control myocyte. Bottom: detubulated myocyte. Transmission images show that myocyte integrity was unaltered by detubulation. *B*, cell capacitance, measured by whole-cell patch clamp. Top: voltage protocol and typical capacitative current records. Bottom: detubulation reduced cell capacitance by $\sim$40% ($n = 10$) compared with control ($n = 14$). Mean values are depicted by larger symbols. *C*, peak Ca^{2+} current density was also reduced in detubulated ($n = 9$) *versus* control ($n = 8$) myocytes. Top: voltage protocol and representative current records on stepping from −40 to 0 mV test potential. *D*, top: transverse line scan images of electrically evoked Ca^{2+} transients (AM-loaded Fluo-3). In control myocytes, the presence of the t-tubular system ensures the spatially homogeneous increase of $[Ca^{2+}]_i$ after an adequate electrical stimulus. T-system disruption causes asynchronous Ca^{2+} release from the sarcoplasmic reticulum, with a smaller and delayed increase of $[Ca^{2+}]_i$ in the centre of the cell. Ca^{2+} transients are shown as the time courses of fluorescence (ratio of fluorescence to background fluorescence, F/F_o) in a sub-sarcolemmal region (periphery) or in the core of the cell. Bottom: global time-to-peak of evoked Ca^{2+} transients in control ($n = 16$) and detubulated ($n = 19$) cells. *E*, volume of control and detubulated myocytes. Length (l) and width (w) measurements were taken from transmission images. Volume was calculated from the equation of an elliptical cylinder, assuming depth (d) = w/3 (see Supplemental Fig. S2 for details of myocyte dimensions). *F*, intrinsic intracellular buffering capacity (β_{int}) of control and detubulated ventricular myocytes, measured by exposing the cells to step-wise decreasing NH_4Cl concentrations of Hepes-buffered Tyrode solution, in the presence of 30 μM cariporide (specimen pH_i traces, control (black) and detubulated (grey) shown in upper panel, along with estimates of β_{int}). Data pooled from 11–15 similar experiments.

flux activity, and a correspondingly smaller peak at lower activity levels.

In summary, stimulation of NHE1 results in H^+ extrusion from both lateral sarcolemma and end regions of the cell (where intercalated discs are most prominent). This leads to global pH_i recovery, but recovery occurs faster in local sub-membranous regions, resulting in spatial pH_i non-uniformity. Both longitudinal and radial pH_i gradients develop during the recovery period, but the former are twice as large as the latter, suggesting that the greater portion of acid extrusion occurs from the ends of the cell. The size of an intracellular pH_i gradient is influenced by the cytoplasmic diffusion distance to membrane transporters, which is greater longitudinally.

Overall, the results of spatial pH_i imaging are consistent with the distribution of NHE1 immunofluorescence and with results of myocyte detubulation, suggesting that NHE1 resides principally in lateral sarcolemma and intercalated discs, with minimal representation in t-tubules.

NHE1 induces pH_i microdomains in CO_2/HCO_3^- buffer, NBC does not. The first trace shown in the right-hand panel of Fig. 5*A* illustrates that a transient longitudinal pH_i gradient (peak end-to-centre gradient of 0.08 units,

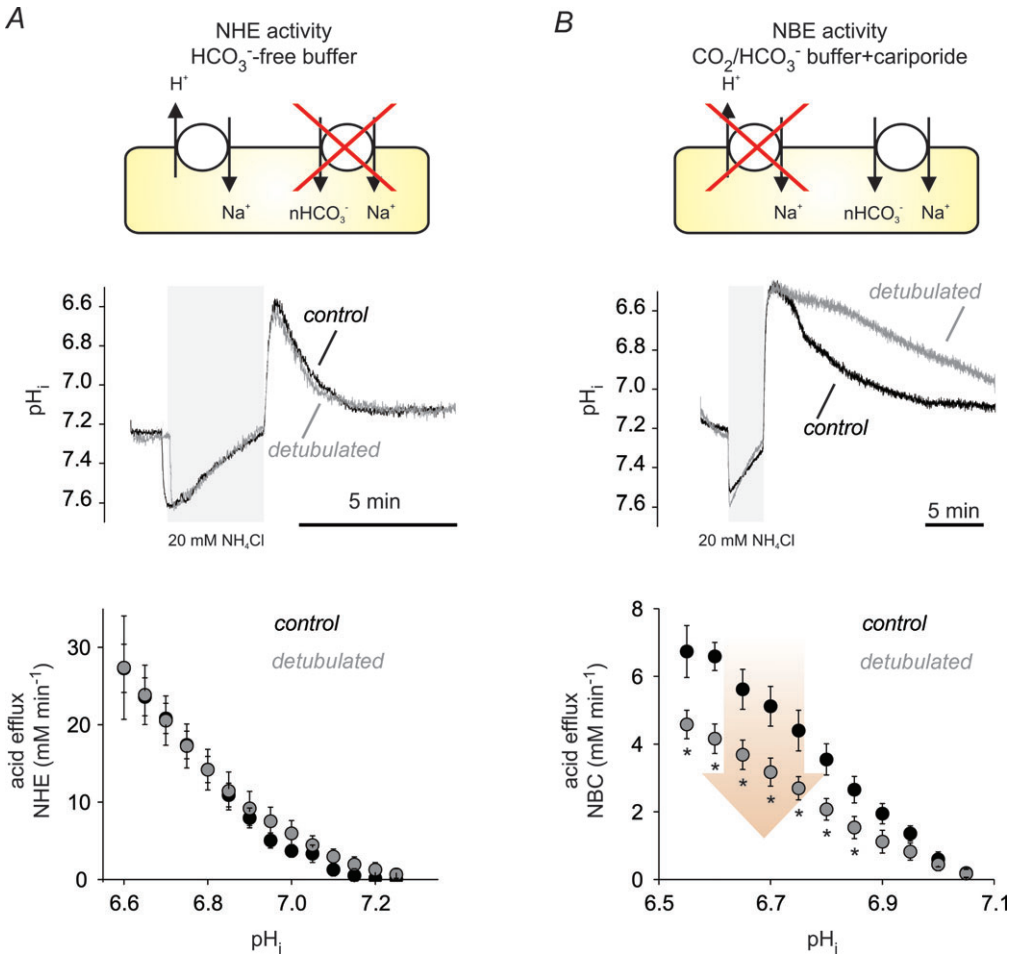

Figure 3. Effect of detubulation on whole-cell NHE1 and NBC activity
pH_i recovery from an acid load mediated via NHE1 is unaffected by detubulation, while recovery via NBC is significantly reduced. *A*, top panel: specimen recording (in black) of pH_i recovery from an intracellular acid load (ammonium prepulse), measured in a control isolated myocyte (pH epifluorescence, whole-cell recording from AM-loaded SNARF-1), superfused with HCO_3^--free, Hepes-buffered solution. Under these conditions, pH_i recovery reflects NHE1 activity. Superimposed grey trace shows a specimen record from a detubulated myocyte, suggesting no effect on pH_i recovery. Bottom panel summarises whole-cell H^+ efflux via NHE1, plotted *versus* pH_i, in control ($n = 12$–21) and detubulated myocytes ($n = 6$–9). *B*, detubulation effect on NBC activity. Top panel: black trace shows a specimen record of pH_i recovery, mediated by NBC, in a cell superfused with HCO_3^-/CO_2-buffered solution, containing 30 μM cariporide (to inhibit NHE1). Grey trace (superimposed) shows specimen pH_i recovery in a detubulated myocyte; recovery is slowed, suggesting loss of NBC activity. Bottom panel: NBC flux activity is plotted *versus* pH_i for control ($n = 5$–7) and detubulated cells ($n = 10$).

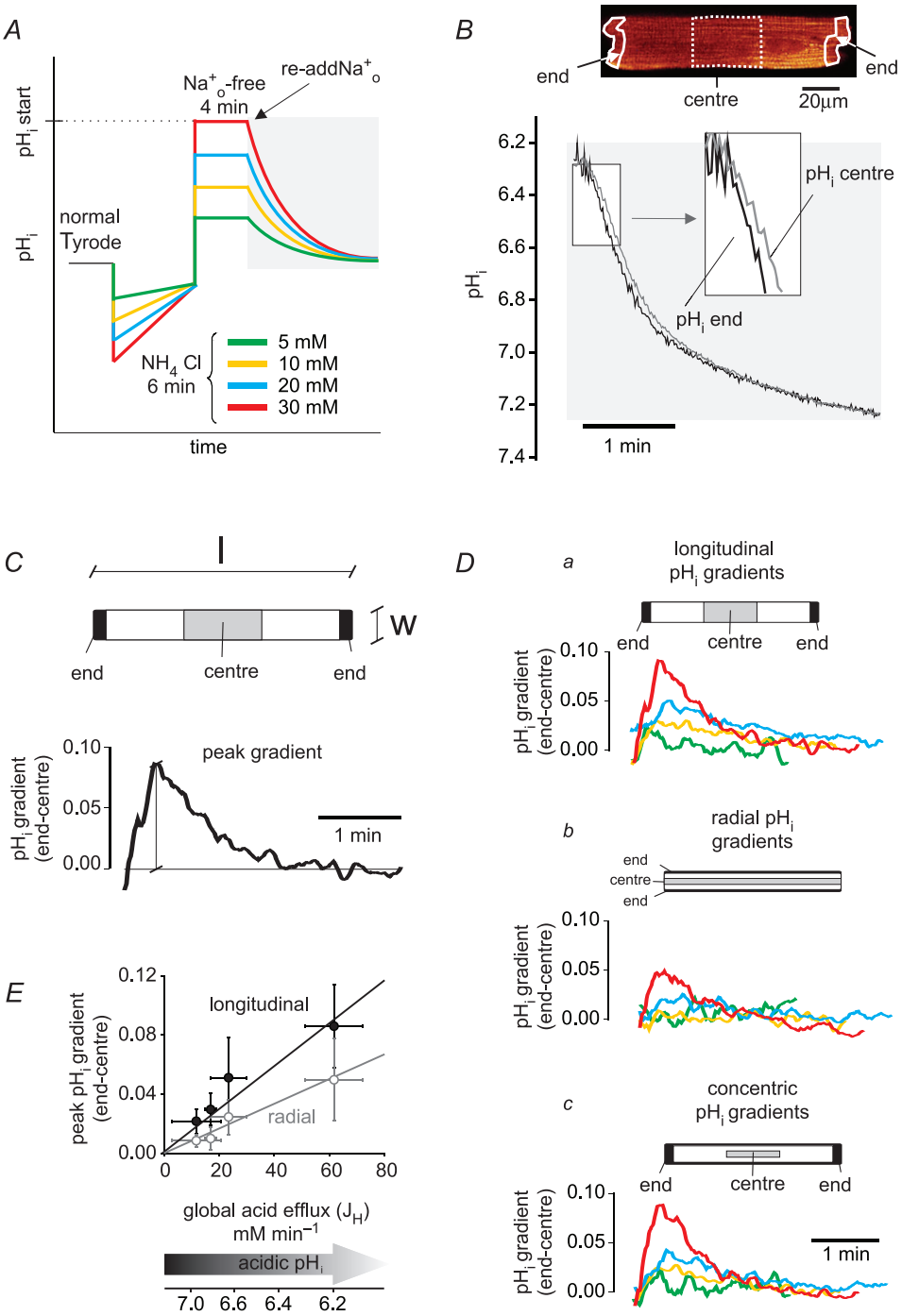

Figure 4. NHE1 activation generates spatial pH$_i$ gradients
A, protocol for inducing spatial pH$_i$ gradients within rat ventricular myocytes. Acid loads of differing magnitude are imposed by prepulsing cells with various concentrations of NH_4Cl (5–30 mM). The pH$_i$ is then clamped at a given acid level by superfusing Na^+-free solution. Upon re-adding Na^+_o, subsequent pH$_i$ recovery occurs via NHE1 (CO_2/HCO_3^--free, Hepes-buffered superfusates). During this phase (grey background) pH$_i$ is confocally imaged (AM-loaded SNARF-1). *B*, cell has been prepulsed with 30 mM NH_4Cl (6 min). Na^+_o re-addition activated pH$_i$ recovery from pH$_i$ 6.25, measured in end and central ROIs, each spanning the width of the cell. Note that pH$_i$ recovered faster in the end ROI (shown at higher resolution in the inset; central ROI recovered with a time delay of ~4 s. As a result, a longitudinal spatial pH$_i$ gradient appeared, quantified in *C* as (pH$_{end}$ – pH$_{centre}$), and plotted *versus* time. Schematic diagram of myocyte shows typical dimensions: 100 μm long (*l*) and 28 μm wide (*w*); end

averaged for 4 cells) was still evident when acid extrusion was activated by Na^+_o re-addition in the presence of 5% CO_2/22 mM HCO_3^- buffer. The similar-sized gradient observed for cells superfused either with Hepes (Fig. 5*A* left panel; averaged for 4 cells; Fig. 5*B*, filled circle) or CO_2/HCO_3^- buffer (Fig. 5*A* right panel; Fig. 5*B*, upper open circle), suggests that the additional intracellular H^+ buffering caused by the presence of CO_2/HCO_3^- must be low. Indeed, the equilibrium value of CO_2-dependent buffering power, β_{CO_2}, is <5 mM at the pH_i values (6.25) where acid efflux was typically reactivated. In contrast, *intrinsic* (non-CO_2) buffering at this pH_i is ∼45 mM (Fig. 2*F*). Thus the additional intracellular buffering due to the presence of CO_2/HCO_3^- would not be expected to suppress pH_i non-uniformity. Intracellular pH microdomains are therefore induced during acid extrusion, even in the presence of physiological CO_2/HCO_3^- buffer.

As both NHE1 and NBC are active in the presence of CO_2/HCO_3^-, while only NHE1 is active in Hepes buffer, the similar sizes of the pH_i gradients observed in the two conditions (Fig. 5*A*) suggests that NHE1 is the principal determinant of spatial pH_i non-uniformity. This was corroborated by the observation (Fig. 5*A*, right panel) that, inhibiting NHE1 activity in CO_2/HCO_3^- buffer (by adding 30 μM cariporide) completely removed the longitudinal pH_i gradients induced when Na^+_o was readmitted. This occurred despite the fact that NBC transporters were reactivated (NBC is cariporide insensitive). Flux data are plotted in Fig. 5*B*, and confirm that the combination of NHE and NBC activity induced a pH_i gradient (filled circle) similar to that observed for NHE1 flux alone (the combined NHE + NBC average flux value lies close to the best-fit grey line for the NHE1 flux data alone).

Global acid efflux values for NBC have also been plotted in Fig. 5*B* (filled triangle and square, 5–15 mM min^{-1}). In one case (triangle) the CO_2/HCO_3^--buffered superfusate contained 4.5 mM K^+_o ($n = 5$), while in the other (square) NBC activity was roughly doubled by raising K^+_o to 45 mM ($n = 6$). An elevated K^+_o depolarises myocyte membrane potential, which stimulates NBCe1, because of the transporter's electrogenicity (Aiello *et al.* 1998; Yamamoto *et al.* 2005). As emphasised in Fig. 5*A* and *B*, neither of these NBC fluxes was associated with any measurable longitudinal or radial pH_i gradient. In contrast, a comparable magnitude of NHE1 flux induced small, but readily measurable longitudinal gradients of ∼0.03 units (Fig. 5*B*). We therefore conclude that pH_i non-uniformity is a consequence of NHE1 activity but not of NBC.

Discussion

Localised expression of sarcolemmal pH-transporters

The present work establishes that NHE1 and NBC, the principal Na^+-dependent acid-extruding transport proteins in the rat ventricular myocyte, differ in their spatial pattern of sarcolemmal expression. NBC (comprising both NBCe1 and NBCn1 isoforms) is trafficked to lateral sarcolemma, intercalated disc membrane, and t-tubules. In contrast, NHE1 is largely excluded from t-tubules. This striking difference correlates with a unique spatial pattern of cellular activity for each transporter type, as illustrated in the schematic diagram of Fig. 6*A*. Following a decrease in pH_i, global acid extrusion is dominated by sarcolemmal H^+ ion efflux on NHE1, as demonstrated in Fig. 3. This efflux is clustered most notably at the ends of the cell where, as discussed later, the geometrical combination of both lateral sarcolemma and intercalated disc membranes results in a high local transporter density. In contrast, because of the lack of NHE1 activity in t-tubules, acid extrusion in these latter regions is dependent on HCO_3^- ion influx via NBC. A comparable spatial pattern for ventricular NHE1 and NBC is likely to operate in other mammalian species, including human, given that the same component transporters have been identified (Leem *et al.* 1999; Yokoyama *et al.* 2000; Loh *et al.* 2002; Yamamoto *et al.* 2005). Indeed, in guinea-pig ventricular myocytes, we have observed universal sarcolemmal immunofluorescence for NBCe1 (including t-tubules and intercalated discs; $n = 14$), but no reduction of NHE1-mediated

ROI length 5 μm (*l*/20); central ROI length 30 μm (6*l*/20). The average distance between end and central ROIs is ∼47.5 μm. *Da*, family of superimposed longitudinal pH_i gradient time courses, obtained by reactivating NHE1 (Na^+_o readdition) from successively less acidic starting levels. NHE1-mediated H^+ efflux is less, the higher the starting pH_i, and is associated with a smaller peak pH_i gradient; *Db*, same protocol, showing family of radial pH_i gradient time courses, measured as (pH_i in sub-sarcolemmal ROI – central ROI). Each ROI, of ∼1.4 μm and ∼8.5 μm wide (sub-sarcolemmal and central, respectively), spans the whole length of cell; average radial distance 13.3 μm; *Dc*, same protocol, showing spatial pH_i gradient time courses measured as (pH_i in concentric, sub-sarcolemmal ROI – pH_i in central ROI), central ROI 30 μm long (6*l*/20) and 8.5 μm wide (6*w*/20). *E*, peak size of longitudinal and radial pH_i gradients *vs.* level of NHE1 activity, measured as global acid efflux (CO_2/HCO_3^--free, Hepes-buffered superfusate). The magnitude of the pH_i gradient increases linearly with NHE1 activity, and is ∼50% smaller for radial gradients; $n = 3$–5. Radial gradients, when normalised to longitudinal gradients obtained from same cell (not shown), were significantly smaller ($P < 0.05$, $n = 3$–5).

acid extrusion after detubulation (pH_i epifluorescence experiments, $n = 5$), identical to the situation in rat myocytes.

Although their expression patterns differ, NHE1 and NBC both contribute to the regulation of cytoplasmic pH (Leem *et al.* 1999; and see Fig. 3). Nevertheless, they may have different *local* functions. For example, because of its co-expression with L-type Ca^{2+} channels in t-tubules (Fig. 1*C*), NBC protein has privileged access to pH_i at the sites of E–C coupling. Activity of L-type Ca^{2+} channels (Saegusa *et al.* 2011), sarcoplasmic reticulum Ca^{2+} release channels (Rousseau & Pinkos, 1990), SERCA pumps (Mandel *et al.* 1982) and NCX (Boyman *et al.* 2011), which are strongly expressed in the vicinity of the t-tubule, are all pH sensitive. In contrast, NHE1 at intercalated discs is co-expressed with Cx43 connexin proteins (Fig. 1*C*), which are the dominant components of ventricular gap junctional channels. These channels are also pH_i sensitive, being biphasically modulated, such that junctional permeability ions current and other solutes is decreased at both low and high pH_i values (Swietach *et al.* 2007*a*). It therefore appears that NBC helps to control pH_i adjacent to the t-tubules, thus guarding E–C coupling (Fig. 6*B*), while NHE1 is the principal guardian of pH_i in gap junctional domains, hence protecting cell-to-cell communication and electrical conduction (Fig. 6*C*). By also contributing to whole-cell cytoplasmic pH_i regulation, both transporters will indirectly influence the contractile proteins, in particular the Ca^{2+}-binding sites on the tnC of the thin filaments, which are pH sensitive (Ca^{2+} binding to tnC is decreased when H^+ ions titrate adjacent troponin I subunits; Ball *et al.* 1994). Thus, NHE1 and NBC proteins are likely to serve both local and global roles in the control of cardiac pH_i.

Given that acid extrusion on NHE1 and NBC proteins is coupled to Na^+ influx, their different spatial distribution will result in a heterogeneous pattern of $[H^+]_i$-gated Na^+ entry into the myocyte. Firstly, as global acid extrusion at low pH_i is significantly less via NBC than NHE1 (Fig. 3), cellular Na^+ loading via NBC will also be less. Secondly, one of the two expressed NBC isoforms, NBCe1, has Na^+-sparing activity, because of its stoichiometric ion coupling of $2HCO_3^-$ with $1Na^+$ (in contrast, NBCn1 and NHE1 have a coupling of $1H^+$ equivalent with $1Na^+$). For these two reasons, total Na^+ entry via generic NBC in the t-tubules will be less than via the combination of NBC and NHE1 in lateral sarcolemma/intercalated disc. The effect of this spatially distributed Na^+ entry on myocyte function has yet to be explored, but it is worth noting that another Na^+-coupled transporter, NCX, is also heterogeneously expressed, being more prevalent in t-tubules than at the lateral sarcolemma (Despa *et al.* 2003). Given that Na^+ influx on transporters such as NHE1 and NBC can be functionally coupled to a rise of intracellular Ca^{2+}, via membrane NCX activity, the lower Na^+ influx in tubular regions may help to reduce the possibility of local cytoplasmic Ca^{2+} overload.

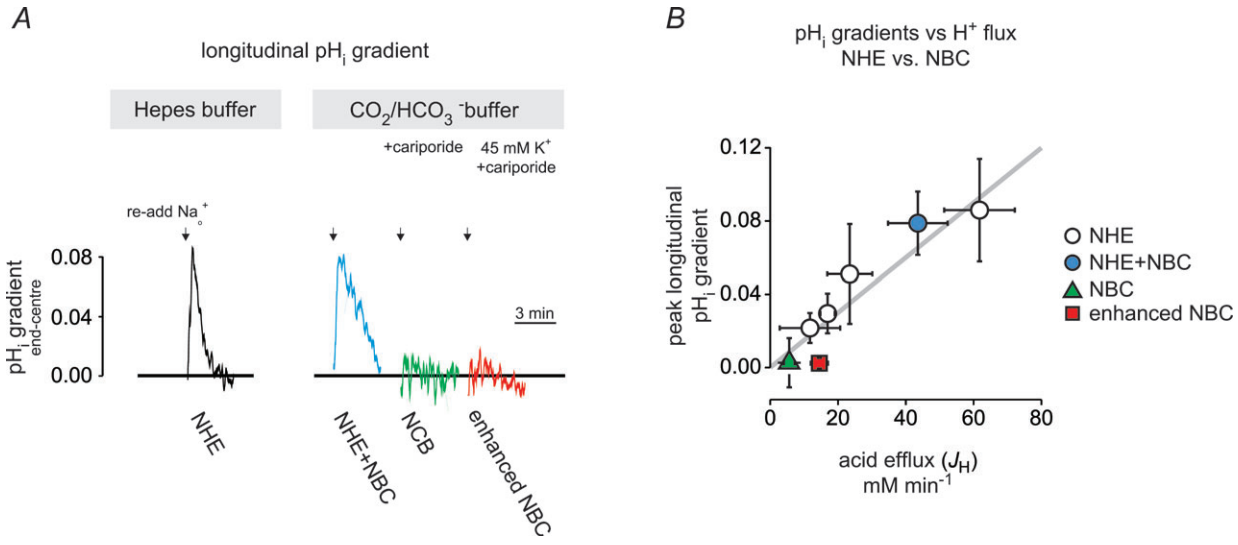

Figure 5. NBC activation does not generate spatial pH_i gradients
A, peak longitudinal pH_i gradients of similar magnitude (induced by Na^+_o re-addition after NH_4Cl prepulse, as in Fig. 4) were observed with Hepes- or CO_2/HCO_3^--buffered superfusates (initial intracellular acid load was similar in both cases, not shown; cells were prepulsed with 30 mM NH_4Cl for 6 min before Na^+_o re-addition). Cariporide (30 μM) abolished pH_i gradient in CO_2/HCO_3^-, even though NBC was still active. With CO_2/HCO_3^- superfusates containing 30 μM cariporide, doubling NBC activity in high $[K^+]_o$ (raised from 4.5 to 45 mM; see main text), failed to evoke a pH_i gradient. *B*, peak longitudinal pH_i gradient ($pH_{end} - pH_{centre}$) is plotted *versus* initial acid-extrusion rate, evoked on Na^+_o re-addition. Peak pH_i gradient increases linearly with magnitude of NHE1-mediated acid extrusion, but no gradient is associated with NBC activity alone ($n = 4$–6).

The strong immunofluorescence signal for NHE1 at intercalated discs (Fig. 1) may reflect high membrane-invagination in these regions, rather than an increased density of protein expression per unit area of membrane. A strong NHE1 expression may seem paradoxical, given that intercalated discs are associated with the abutment of adjacent myocytes, which might be assumed to restrict carrier activity. The functional efficiency of NHE1 within intact myocardium has yet to be assessed, but the proximity of other cells need not present an insurmountable barrier. Even with extensive membrane infolding, transport proteins can still have access to adequate flux pathways, especially for small extracellular solutes such as H^+ and Na^+ ions. Indeed, the present work shows that, in the isolated myocyte, high membrane tortuosity at the ends of the cell or in the t-tubules does not preclude acid extrusion via NHE1 or NBC. It remains to be seen, however, whether tubular NBC activity requires the presence of exofacial carbonic anhydrase molecules, to facilitate local CO_2 or H^+ ion diffusion, as suggested for membrane acid extrusion into the t-tubules of skeletal muscle (Hallerdei *et al.* 2010).

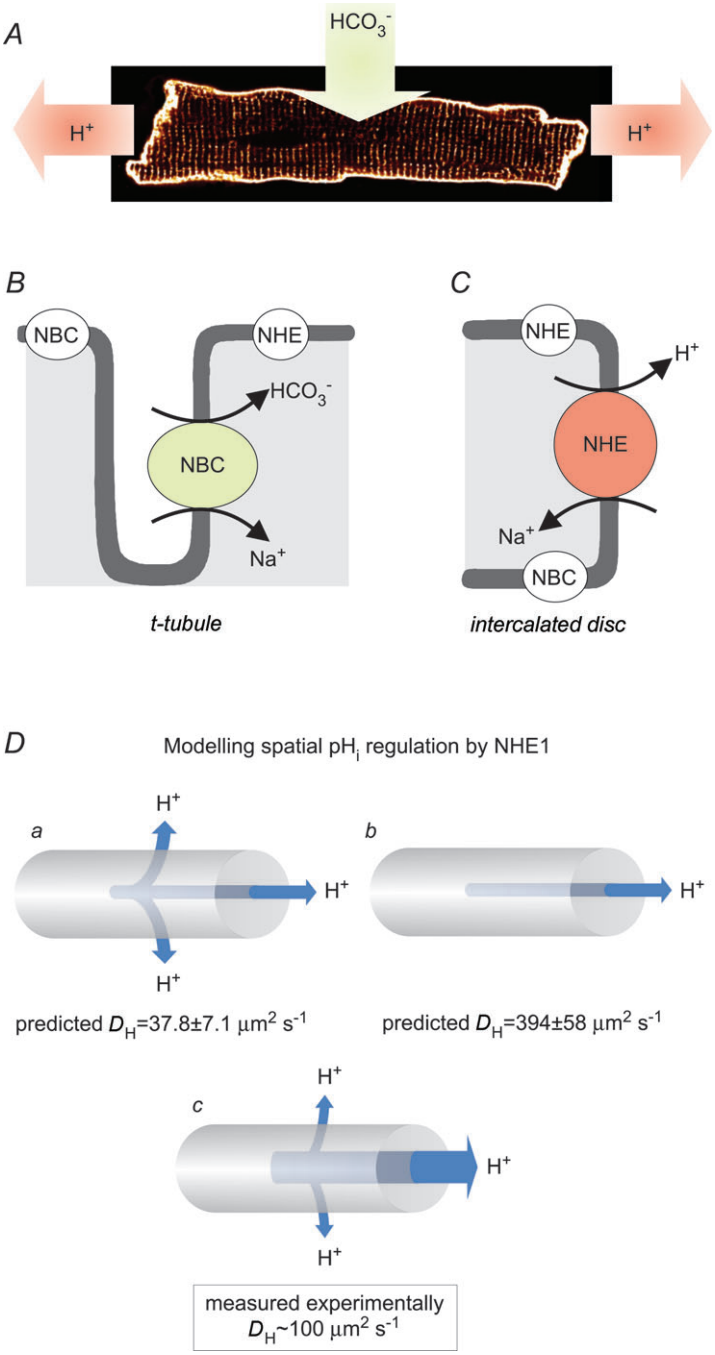

Figure 6. Local control of pH_i
A, NBCe1 and NBCn1 (i.e. generic NBC), but not NHE1, are expressed in t-tubules. Therefore HCO_3^- influx via NBC mediates acid extrusion in these regions (represented by downward arrow). Both NBC and NHE1 are expressed in lateral sarcolemma and intercalated disc regions, but acid efflux via NHE1 > NBC. Thus H^+ efflux predominates, and this is more evident at the ends of the myocyte, where lateral sarcolemma converges with intercalated disc membrane (represented by horizontal arrows). *B*, local pH_i control by NBC in t-tubules. NBC preferentially guards pH_i in the vicinity of dyadic spaces where E–C coupling proteins reside. *C*, local pH_i control by NHE1 predominates close to gap junctional channels at intercalated disc regions. *D*, modelling NHE1 fluxes that dominate pH_i control in lateral sarcolemma/intercalated discs. Two versions of 3-dimensional, H^+ extrusion model (see main text of Discussion and Appendix) used to simulate spatial pH_i gradient formation during NHE1 activity. *Da*, NHE1 (and hence H^+ ion efflux) with a homogeneous flux density in lateral sarcolemma and intercalated discs; *Db*, NHE1 in intercalated discs only. Models are solved to give best-fit value for D_H (apparent H^+_i mobility coefficient, as indicated). *Dc*, the actual value for D_H (100 $\mu m^2\ s^{-1}$), measured independently in previous work, implies an NHE1 distribution with a higher density of flux activity at intercalated discs relative to lateral sarcolemma.

Comparison with previous reports of pH-transporter expression

NHE1. Previous immunofluorescence mapping has led to mixed reports for NHE1 distribution in ventricular myocytes, with some suggesting a strong presence in t-tubules as well as intercalated discs (Petrecca *et al.* 1999; Lawrence *et al.* 2010), and another suggesting expression mainly at the latter (Snabaitis *et al.* 2006). No previous work, however, has attempted to correlate immunofluorescence staining with spatial measurements of NHE1 transporter activity. Staining alone must always be open to question, because of problems with antibody selectivity, local fluorescence intensity and protocols for antibody application. In the present work, NHE1 staining accords well with dynamic spatial patterns of cytoplasmic pH, i.e. pronounced longitudinal pH_i gradients and more modest radial pH_i gradients when NHE1 is stimulated. As discussed in the next section, these gradients are consistent with H^+ efflux confined to the lateral sarcolemma and intercalated discs. Minimal t-tubular expression is further supported by the lack of effect of physical detubulation on whole-cell NHE1 flux (Fig. 3). The functional evidence thus lends credence to the present NHE1 staining. Finally, even though some residual NHE1 expression may be detected by immunofluorescence in the t-tubules, the present work indicates that its functional activity in these regions is negligible.

A recent report suggests that NHE1 expression levels in ventricular myocytes may be labile, increasing after cellular stress or short periods of contractile activity (Lawrence *et al.* 2010). In this case the NHE1 expression pattern may depend on the history of the cell. However, we have observed a similar pattern for NHE1 (i.e. lateral sarcolemma plus intercalated disc, with little or no t-tubular expression), in both quiescent and electrically paced myocytes (Supplemental Fig. S3), suggesting that NHE1 exclusion from t-tubules is a general expression pattern.

NBC. Although functional evidence for generic NBC activity has been well documented in cardiac tissue and isolated ventricular myocytes, based on recordings of pH_i (Dart & Vaughan-Jones, 1992; Lagadic-Gossmann *et al.* 1992), the isoforms involved have been less well defined. Acid extrusion via generic NBC displays some voltage sensitivity (Camilion de Hurtado *et al.* 1995; Aiello *et al.* 1998; Yamamoto *et al.* 2005), consistent with the presence of an electrogenic isoform, and immunofluorescence has identified general sarcolemmal and t-tubular expression for electrogenic NBCe1 (De Giusti *et al.* 2011), in line with the present findings. The expression of NBCn1, an electroneutral isoform, has proved more controversial. Although protein for NBCn1 has previously been identified by Western blotting of whole-heart samples (Damkier *et al.* 2006), contamination from non-myocyte sources could not be excluded. A histochemical 'gene trap' technique, which monitors promoter activity of the NBCn1 gene, detected transcription in murine atrial but not ventricular tissue (Boedtkjer *et al.* 2008). The technique, however, had the unwanted side-effect of reducing overall protein expression, so assay resolution may have been inadequate for ventricular detection. In further functional work, pH_i measurements in voltage-clamped ventricular myocytes identified both voltage-sensitive and voltage-insensitive components of NBC-mediated acid efflux, ascribed to electrogenic and electroneutral isoforms, respectively (Yamamoto *et al.* 2005). The present work is thus consistent with this latter conclusion, as membrane expression of both NBCe1 and NBCn1 has now been detected by immunofluorescence. Furthermore, Western blotting detects a single band for NBCn1 and clear bands for NBCe1, specifically from enzymically isolated ventricular myocytes (Fig. 1*A*). In summary, it seems likely that both electrogenic (NBCe1) and electroneutral (NBCn1) isoforms are expressed in ventricular myocytes, and that they are trafficked to surface sarcolemma, intercalated discs and t-tubular regions. Expression of NBCe2, however, is questionable, as clear trafficking to sarcolemmal membrane regions was not evident in the present work (Supplemental Fig. S1).

Cl^-/HCO_3^- exchange and MCT. Immunofluorescence mapping has been reported previously for other types of pH-transporter in cardiac myocytes, including Cl^-/HCO_3^- exchange (gene products Slc4a1, Slc4a3 and Slc26a6, transporters that mediate acid *influx* into myocytes; Alvarez *et al.* 2007), and MCT-1 (Slc16, a lactate transporter that is recruited during periods of high glycolytic activity; Halestrap *et al.* 1997). In all cases, expression was seen in lateral sarcolemma and intercalated disc regions but only Slc4a3 and Slc26a6 mapped to the t-tubules. These distribution patterns, however, have yet to be confirmed functionally in confocal pH_i imaging or detubulation experiments, although tubular MCT activity was mooted in early non-confocal imaging work (Halestrap *et al.* 1997). The spatial patterns of Cl^-/HCO_3^- exchange and MCT must therefore be regarded as provisional, particularly with respect to the functional implications.

pH_i microdomains: formation and functional relevance

Induction of pH_i microdomains. The present work demonstrates that expression of NHE1 in lateral sarcolemma and intercalated discs is associated with spatial pH_i heterogeneity. It is instructive to consider why this should be. Under resting conditions cytoplasmic pH is

essentially uniform (Vaughan-Jones *et al.* 2002), but when acid extrusion is stimulated by a fall of bulk pH_i, H^+ efflux on NHE1 will cause sub-membranous acid-depletion, thereby triggering H^+ diffusion into the depleted zone from regions deeper within the cell. The magnitude of the resulting longitudinal and radial $H^+{}_i$ gradients will depend partly on $H^+{}_i$ mobility. As this is naturally low, large and relatively long-lived spatial gradients may form (up to ∼0.1 pH_i units in magnitude over a 50 μm longitudinal distance, and lasting for >2 min, see Fig. 4). As shown in Fig. 5, the gradients subside as sarcolemmal H^+ efflux decreases, following bulk pH_i recovery to a more alkaline level. Cytoplasmic H^+ mobility is restricted by the high capacity of H^+ buffer sites on intracellular proteins that are poorly mobile (Vaughan-Jones *et al.* 2002; Zaniboni *et al.* 2003). Spatial H^+ movement occurs, not via free H^+ ion diffusion, but via reversible H^+ binding to smaller buffer molecules that diffuse more readily, liberating their H^+ ions in less acidic regions. These molecules comprise histidyl dipeptides (HDPs) such as carnosine, anserine and homocarnosine (with a combined intracellular concentration of ∼17 mM), and, to a more limited extent, CO_2/HCO_3^- molecules (Vaughan-Jones *et al.* 2002; Swietach *et al.* 2007*b*, 2010). Because of their intermediate molecular weight (200–250 Da), HDPs diffuse at only a modest rate, which results in an apparently low $H^+{}_i$ mobility. Low mobility, when combined with high membrane H^+ efflux, and relatively long cytoplasmic diffusion distances to the NHE1 transporters (14–50 μm in the myocyte), disposes the cell to spatial $H^+{}_i$ gradients.

$H^+{}_i$ mobility can be estimated from the time delay, t, for a pH_i rise in different cytoplasmic regions following stimulation of NHE1 activity. In experiments similar to those shown in Fig. 4*B*, this delay was 3.74 ± 0.68 s ($n = 12$) for recovery at pH_i ∼6.9 in 'end' *versus* 'central' myocyte regions (see inset), separated by ∼50 μm. Using a 3-D diffusion model (Swietach & Vaughan-Jones, 2005*b*), it is possible to derive an apparent H^+ diffusion coefficient (D_H) corresponding to this delay. Assuming that NHE1 flux density is distributed homogeneously in lateral sarcolemma and intercalated discs, as represented by the sides and ends, respectively, of a simple cylinder (Fig. 6*Da*), the best-fit value of D_H to the measured time delay is 37.8 ± 7.1 $\mu m^2\ s^{-1}$. If, instead, all NHE1 activity is assumed to be concentrated at the intercalated disc regions, with no expression in lateral sarcolemma (Fig. 6*Db*), then the best-fit D_H becomes 394 ± 58 $\mu m^2\ s^{-1}$. Further details of the model are presented in the Appendix to this paper. Intracellular D_H has previously been measured directly in experiments where $H^+{}_i$ diffusion gradients were set up in ventricular myocytes, using H^+ ion micro-injection (Vaughan-Jones *et al.* 2002; Swietach *et al.* 2003; Zaniboni *et al.* 2003), photolytic H^+ uncaging (Swietach *et al.* 2007*b*, 2010), or local exposure to membrane-permeant weak acids/bases (Swietach & Vaughan-Jones, 2005*a*). Overall, these experimental approaches estimated D_H to be in the region of 100 $\mu m^2\ s^{-1}$ (at pH_i 6.9), a value close to the present D_H model estimate assuming NHE1 activity in lateral sarcolemma/intercalated discs (Fig. 6*Da*). Indeed, as described in the Appendix, the best model fit, using previously determined values for D_H, is likely to correspond to a lateral sarcolemmal expression of NHE1, combined with a somewhat higher expression density at intercalated discs (Fig. 6*Dc*), a prediction that matches the higher level of NHE1 immunofluorescence staining observed in these latter regions (Fig. 1). Localisation of NHE1 in the above two surface membrane domains is also in agreement with earlier model predictions (Swietach & Vaughan-Jones, 2005*b*). Thus mathematical simulation, pH_i spatial imaging, immunofluorescence staining and detubulation protocols all support a surface expression of NHE1 and a lack of activity in t-tubules.

One may ask why spatial pH_i non-uniformity was not seen during NBC stimulation. Because of its location on t-tubular as well as lateral sarcolemma/intercalated disc membranes, diffusion distances from any cytoplasmic region to an NBC protein will be no more than a couple of micrometres. Using a value of 100 $\mu m^2\ s^{-1}$ for D_H, the Einstein equation for diffusion predicts a cytoplasmic time delay, t, of 20 ms for H^+ ion passage over a 2 μm distance, x, to a transporter (where $t = x^2/2D_H$). Such a brief time delay cannot be resolved using present experimental techniques. Given their spatial distribution, and assuming an even level of membrane expression, NBCs are thus unlikely to induce significant pH_i non-uniformity, at least not on a time scale of seconds or minutes, as observed experimentally. The same argument can be used to address the possible location of NHE1 in t-tubules. If activity were present there, global pH_i would be expected to appear uniform during stimulation of NHE1, a result that was *not* observed experimentally, confirming the functional absence of transporter from this region.

It is difficult to reconcile the present results with a recent report for major pH_i gradients developing on the nanometer spatial scale, local to Cl^-/HCO_3^- ion transporter proteins (anion exchanger 1 (AE1), gene product Slc4a1), when these were heterologously expressed in cells of the human embryonic kidney cell line (HEK) (Johnson & Casey, 2011). Stimulation of acid extrusion on AE1 appeared to induce a pH_i rise in the vicinity of an adjacent plasmalemmal marker protein, positioned 50 nm away, but with a time delay of 6 s. On a simple diffusion model, this large delay over such a short distance would indicate an apparent H^+ mobility of 2.08×10^{-4} $\mu m^2\ s^{-1}$, again derived from the Einstein equation. This value is 0.5 *million* times lower than that estimated in cardiac myocytes. Such low mobility (10^4 times lower than typical protein mobility) would suggest essentially no cytoplasmic diffusive coupling between the two membrane proteins,

despite comparable pH_i changes being observed at both sites. Bulk cytoplasmic H^+ mobility is not consistent with this paradoxical H^+ ion behaviour. Indeed, the possibility must remain that kinetic differences among the various protein-linked pH reporter dyes (Mallik *et al.* 2003), as used in the HEK cell experiments, may account for the temporal pH differences. Whatever the explanation, the ultra-slow H^+ movement suggested on the nanometer scale is clearly not equivalent to the more moderate mobility measured on the micrometre scale in cardiac myocytes, and estimated in other cell types (Swietach *et al.* 2003), including epithelial cells and invertebrate/mammalian neurons.

Functional importance of pH_i microdomains. The functional implications of pH_i microdomain formation during pH_i regulation have yet to be fully assessed. In ventricular myocytes, given the high H^+ ion sensitivity of intracellular contractile and Ca^{2+}-handling proteins, local pH differences of up to 0.1 pH units would be expected to modulate active tension generated by sarcomeres positioned in different regions of the cell (note that a global pH_i decrease of 0.1 units can reduce whole-cell contraction by up to 25%; as shown in Fig. 7 of Vaughan-Jones *et al.* (2009)). Intracellular pH gradients have also been shown to influence the spatial distribution of diastolic and systolic Ca^{2+} (Swietach *et al.* 2012, 2013), and would be expected to modulate the activity of other spatially distributed Ca^{2+}-handling proteins, such as NCX and the L-type Ca^{2+} channel. Overall, a cytoplasmic pH non-uniformity runs the risk of desynchronising the mechanical and chemical signalling activity of a cardiac cell, unless local compensatory mechanisms are rapidly brought into play. The pH_i microdomains reported in the present work are particularly evident during high NHE1 activity, which coincides with global intracellular acidosis. The break-up of a spatially uniform cytoplasmic pH may therefore contribute to the well-known arrhythmogenic and injurious effects of acidosis in the heart. This may be particularly relevant to ventricular myocytes in failing hearts, where NHE activity is found to be increased (Yokoyama *et al.* 2000).

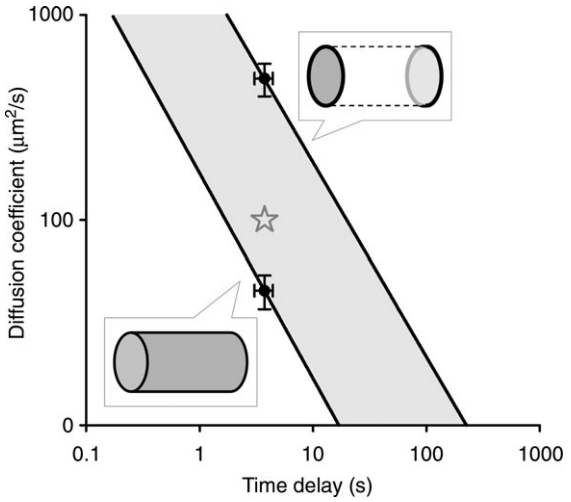

Figure 7. Simulated relationship between time delay and H^+ diffusion coefficient
The mathematical model of acid extrusion by NHE1 was run for a range of H^+ diffusion coefficients to derive the time delay between simulated pH_i recovery time courses at the cell centre and cell ends. The relationship between time delay and H^+ diffusion coefficient was simulated for two cases of NHE1 activity distribution: uniform over surface sarcolemma and intercalated disc membranes (*A*), and confined to intercalated disc membrane (*B*). The experimentally derived time delay of 3.74 ± 0.68 s corresponds to a diffusion coefficient of 37.8 ± 7.1 μm^2 s^{-1} for uniform NHE1 distribution and 394 ± 58 μm^2 s^{-1} for intercalated disc-confined NHE1. The actual H^+ diffusion coefficient, measured in independent experiments, is 100 μm^2 s^{-1} (denoted by star symbol).

Local pH_i regulation through spatially distributed pH-transporter expression need not be unique to the cardiac myocyte. Induction of transient pH_i microdomains has also been reported for epithelial cells (duodenal enterocytes) (Stewart *et al.* 1999), migrating tumour cells (Martin *et al.* 2011), and neurons (Schwiening & Willoughby, 2002; Willoughby & Schwiening, 2002). In enterocytes and migrating tumour cells, pH microdomain induction is clearly favoured by polarisation of membrane pH-transporter expression (e.g. in enterocytes, H^+-coupled dipeptide transporters are confined to the apical membrane). In neurons, with the polymorphism of cell body, dendritic tree and presynaptic terminals, mathematical modelling predicts spatial pH_i gradients, even with uniformly expressed pH-transporters (Swietach *et al.* 2003). Nevertheless, membrane localisation of these carriers, or of other H^+-coupled ion pumps such as the plasmalemmal Ca^{2+}-ATPase (which counter-transports Ca^{2+} and H^+ ions), will introduce an additional level of complexity. Spatial pH_i imaging, combined with immunofluorescence mapping and mathematical modelling, as demonstrated in the present work, now provides a powerful means of elucidating local pH_i control.

Conclusions

Na^+-dependent pH-transporters in the ventricular myocyte, NHE1 and NBC, display different spatial patterns of sarcolemmal expression, which may reflect distinct local roles. Thus, as well as globally regulating pH_i, NHE1 at intercalated discs controls $[H^+]_i$ in the vicinity of gap junctions, thus helping to regulate cell-to-cell electrical and chemical continuity, while NBC in t-tubules influences $[H^+]_i$ close to Ca^{2+}-handling proteins responsible for E–C coupling. Local pH_i control is accentuated by a low cytoplasmic H^+ ion mobility, which can lead to long-lived pH_i microdomains. Given

that spatial remodelling of gap junctions and t-tubules is a major symptom of disease states such as cardiac hypertrophy and heart failure (Wei *et al.* 2010; Chkourko *et al.* 2012; Sachse *et al.* 2012), it will be of considerable interest to determine if these clinical disorders are also linked to a spatial remodelling of pH-transporter distribution and function.

Appendix

Modelling intracellular spatial H^+ ion dynamics

The spatio-temporal behaviour of intracellular $[H^+]$ during acid-extrusion by NHE1 was simulated in a model myocyte of cylindrical symmetry, as previously described (Swietach & Vaughan-Jones, 2005*b*) (length 100 μm, radius 14 μm). For the purpose of plotting pH_i time courses, the cell was divided into twenty cylindrical regions of interest (ROIs) along its length. The surface membrane was assumed to be smooth (i.e. no invaginations) because NHE1 is not present in the t-system. The intracellular buffering capacity was derived from previous work (Zaniboni *et al.* 2003). The pH_i sensitivity of NHE1 flux was given by a Hill equation (Yamamoto *et al.* 2005):

$$J = J_{\max} \frac{[H^+]^n}{[H^+]^n + K^n}$$

Cooperativity (n) was 1.933, affinity constant (K) was $10^{-6.38}$ M, and maximal flux ($J_{\max}$) was 34.188 mM min^{-1}.

Two cases of NHE1 activity distribution were simulated. In the first case, NHE1 activity was assumed to be uniform per unit area of membrane over the lateral sarcolemma (sides) and intercalated disc (ends). In the second case, NHE1 activity was confined to the intercalated disc membrane. To account for the absence of NHE1 in the lateral sarcolemma, $J_{\max}$ for NHE1 at the intercalated disc membrane was scaled by a factor of 8.14 (= total area of cell/area of intercalated discs). The apparent intracellular H^+ diffusion coefficient (D_H) was varied from 10 to 1000 $\mu m^2\ s^{-1}$. Starting pH_i was set to 6.6. Simulated pH_i recovery time courses were sampled in the cell centre (average of six central ROIs) and cell ends (average of 1st and 20th ROI). The time delay between pH_i recovery time courses at the cell centre and cell ends was calculated when cell-averaged pH_i reached 6.9.

The relationship between D_H and time delay is plotted in Fig. 7. For both simulated conditions, the model outputs predict that time delay will increase as D_H is reduced, and that the relationship will be displaced to the right if NHE1 activity is located only at the ends of the cell. The typical experimentally measured value of D_H (100 $\mu m^2\ s^{-1}$) has been plotted (open star) *versus* the mean time delay determined in the present work (see Results). Filled circles show mean D_H values deduced from the two model conditions, again using experimentally measured time delays. Note that the experimentally measured value for D_H falls between those deduced for the two model conditions (although it lies closer to the low deduced value). This indicates that a higher NHE1 expression density at the intercalated discs, coupled with a lower lateral sarcolemmal density will provide the best model fit to the experimentally determined value for D_H.

Simplifying the computational model to cylindrical geometry implies that intercalated discs reside exclusively at the ends of a myocyte. In reality, cell geometry is frequently more complex than this. Several intercalated disc regions, containing higher intensity immunofluorescence for NHE1, may be distributed along the length of an individual myocyte (see e.g. top left panel of Supplemental Fig. S3). Nevertheless, the present simulations illustrate how local pH_i time delays imply that NHE1 is expressed in both lateral sarcolemma and intercalated disc, most likely at different functional levels.

References

Aiello EA, Petroff MG, Mattiazzi AR & Cingolani HE (1998). Evidence for an electrogenic Na^+–HCO_3^- symport in rat cardiac myocytes. *J Physiol* **512**, 137–148.

Alvarez BV, Kieller DM, Quon AL, Robertson M & Casey JR (2007). Cardiac hypertrophy in anion exchanger 1-null mutant mice with severe hemolytic anemia. *Am J Physiol Heart Circ Physiol* **292**, H1301–H1312.

Ball KL, Johnson MD & Solaro RJ (1994). Isoform specific interactions of troponin I and troponin C determine pH sensitivity of myofibrillar Ca^{2+} activation. *Biochemistry* **33**, 8464–8471.

Boedtkjer E, Praetorius J, Fuchtbauer EM & Aalkjaer C (2008). Antibody-independent localization of the electroneutral Na^+-HCO_3^- cotransporter NBCn1 (slc4a7) in mice. *Am J Physiol Cell Physiol* **294**, C591–C603.

Boyett MR, Frampton JE & Kirby MS (1991). The length, width and volume of isolated rat and ferret ventricular myocytes during twitch contractions and changes in osmotic strength. *Exp Physiol* **76**, 259–270.

Boyman L, Hagen BM, Giladi M, Hiller R, Lederer WJ & Khananshvili D (2011). Proton-sensing Ca^{2+} binding domains regulate the cardiac Na^+/Ca^{2+} exchanger. *J Biol Chem* **286**, 28811–28820.

Brette F, Komukai K & Orchard CH (2002). Validation of formamide as a detubulation agent in isolated rat cardiac cells. *Am J Physiol Heart Circ Physiol* **283**, H1720–H1728.

Brette F & Orchard C (2003). T-tubule function in mammalian cardiac myocytes. *Circ Res* **92**, 1182–1192.

Brette F, Salle L & Orchard CH (2006). Quantification of calcium entry at the T-tubules and surface membrane in rat ventricular myocytes. *Biophys J* **90**, 381–389.

Camilion de Hurtado MC, Perez NG & Cingolani HE (1995). An electrogenic sodium-bicarbonate cotransport in the regulation of myocardial intracellular pH. *J Mol Cell Cardiol* **27**, 231–242.

Chkourko HS, Guerrero-Serna G, Lin X, Darwish N, Pohlmann JR, Cook KE, Martens JR, Rothenberg E, Musa H & Delmar M (2012). Remodeling of mechanical junctions and of microtubule-associated proteins accompany cardiac connexin43 lateralization. *Heart Rhythm* **9**, 1133–1140 e6.

Choi HS, Trafford AW, Orchard CH & Eisner DA (2000). The effect of acidosis on systolic Ca^{2+} and sarcoplasmic reticulum calcium content in isolated rat ventricular myocytes. *J Physiol* **529**, 661–668.

Damkier HH, Nielsen S & Praetorius J (2006). An anti-NH_2-terminal antibody localizes NBCn1 to heart endothelia and skeletal and vascular smooth muscle cells. *Am J Physiol Heart Circ Physiol* **290**, H172–H180.

Dart C & Vaughan-Jones RD (1992). Na^+–HCO_3-symport in the sheep cardiac Purkinje fibre. *J Physiol* **451**, 365–385.

De Giusti VC, Orlowski A, Villa-Abrille MC, de Cingolani GE, Casey JR, Alvarez BV & Aiello EA (2011). Antibodies against the cardiac sodium/bicarbonate co-transporter (NBCe1) as pharmacological tools. *Br J Pharmacol* **164**, 1976–1989.

Delmar M & Sorgen P (2009). Molecular organization and regulation of the cardiac gap juntion channel connexin 43. In *Cardiac Electrophysiology. From Cell to Bedside*, 5th edn, ed. Zipes DP & Jalife J, pp. 85–92. Elsevier, Saunders, Philadelphia.

Despa S, Brette F, Orchard CH & Bers DM (2003). Na/Ca exchange and Na/K-ATPase function are equally concentrated in transverse tubules of rat ventricular myocytes. *Biophys J* **85**, 3388–3396.

Elliott AC, Smith GL, Eisner DA & Allen DG (1992). Metabolic changes during ischaemia and their role in contractile failure in isolated ferret hearts. *J Physiol* **454**, 467–490.

Halestrap AP, Wang X, Poole RC, Jackson VN & Price NT (1997). Lactate transport in heart in relation to myocardial ischemia. *Am J Cardiol* **80**, 17A–25A.

Hallerdei J, Scheibe RJ, Parkkila S, Waheed A, Sly WS, Gros G, Wetzel P & Endeward V (2010). T tubules and surface membranes provide equally effective pathways of carbonic anhydrase-facilitated lactic acid transport in skeletal muscle. *PLoS One* **5**, e15137.

Johnson DE & Casey JR (2011). Cytosolic H^+ microdomain developed around AE1 during AE1-mediated Cl^-/HCO_3^- exchange. *J Physiol* **589**, 1551–1569.

Lagadic-Gossmann D, Buckler KJ & Vaughan-Jones RD (1992). Role of bicarbonate in pH recovery from intracellular acidosis in the guinea-pig ventricular myocyte. *J Physiol* **458**, 361–384.

Lawrence SP, Holman GD & Koumanov F (2010). Translocation of the Na^+/H^+ exchanger 1 (NHE1) in cardiomyocyte responses to insulin and energy-status signalling. *Biochem J* **432**, 515–523.

Leem CH, Lagadic-Gossmann D & Vaughan-Jones RD (1999). Characterization of intracellular pH regulation in the guinea-pig ventricular myocyte. *J Physiol* **517**, 159–180.

Loh SH, Jin JS, Tsai CS, Chao CM, Chiung CS, Chen WH, Lin CI, Chuang CC & Wei J (2002). Functional evidence for intracellular acid extruders in human ventricular myocardium. *Jpn J Physiol* **52**, 277–284.

Mallik R, Udgaonkar JB & Krishnamoorthy G (2003). Kinetics of proton transfer in a green fluorescent protein: A laser-induced pH jump study. *Proc Indian Acad Sci (Chem Sci)* **115**, 307–317.

Mandel F, Kranias EG, Grassi de Gende A, Sumida M & Schwartz A (1982). The effect of pH on the transient-state kinetics of Ca^{2+}-Mg^{2+}-ATPase of cardiac sarcoplasmic reticulum. A comparison with skeletal sarcoplasmic reticulum. *Circ Res* **50**, 310–317.

Martin C, Pedersen SF, Schwab A & Stock C (2011). Intracellular pH gradients in migrating cells. *Am J Physiol Cell Physiol* **300**, C490–C495.

Orchard CH & Cingolani HE (1994). Acidosis and arrhythmias in cardiac muscle. *Cardiovasc Res* **28**, 1312–1319.

Petrecca K, Atanasiu R, Grinstein S, Orlowski J & Shrier A (1999). Subcellular localization of the Na^+/H^+ exchanger NHE1 in rat myocardium. *Am J Physiol Heart Circ Physiol* **276**, H709–H717.

Pushkin A, Abuladze N, Newman D, Lee I, Xu G & Kurtz I (2000). Cloning, characterization and chromosomal assignment of NBC4, a new member of the sodium bicarbonate cotransporter family. *Biochim Biophys Acta* **1493**, 215–218.

Rousseau E & Pinkos J (1990). pH modulates conducting and gating behaviour of single calcium release channels. *Pflugers Arch* **415**, 645–647.

Sachse FB, Torres NS, Savio-Galimberti E, Aiba T, Kass DA, Tomaselli GF & Bridge JH (2012). Subcellular structures and function of myocytes impaired during heart failure are restored by cardiac resynchronization therapy. *Circ Res* **110**, 588–597.

Saegusa N, Moorhouse E, Vaughan-Jones RD & Spitzer KW (2011). Influence of pH on Ca^{2+} current and its control of electrical and Ca^{2+} signaling in ventricular myocytes. *J Gen Physiol* **138**, 537–559.

Schmitt BM, Biemesderfer D, Romero MF, Boulpaep EL & Boron WF (1999). Immunolocalization of the electrogenic Na^+-HCO_3^- cotransporter in mammalian and amphibian kidney. *Am J Physiol Renal Physiol* **276**, F27–F38.

Schwiening CJ & Willoughby D (2002). Depolarization-induced pH microdomains and their relationship to calcium transients in isolated snail neurones. *J Physiol* **538**, 371–382.

Snabaitis AK, D'Mello R, Dashnyam S & Avkiran M (2006). A novel role for protein phosphatase 2A in receptor-mediated regulation of the cardiac sarcolemmal Na^+/H^+ exchanger NHE1. *J Biol Chem* **281**, 20252–20262.

Stewart AK, Boyd CA & Vaughan-Jones RD (1999). A novel role for carbonic anhydrase: cytoplasmic pH gradient dissipation in mouse small intestinal enterocytes. *J Physiol* **516**, 209–217.

Swietach P, Camelliti P, Hulikova A, Kohl P & Vaughan-Jones RD (2010). Spatial regulation of intracellular pH in multicellular strands of neonatal rat cardiomyocytes. *Cardiovasc Res* **85**, 729–738.

Swietach P, Rossini A, Spitzer KW & Vaughan-Jones RD (2007*a*). H^+ ion activation and inactivation of the ventricular gap junction: a basis for spatial regulation of intracellular pH. *Circ Res* **100**, 1045–1054.

Swietach P, Spitzer KW & Vaughan-Jones RD (2007*b*). pH-dependence of extrinsic and intrinsic H^+-ion mobility in the rat ventricular myocyte, investigated using flash photolysis of a caged-H^+ compound. *Biophys J* **92**, 641–653.

Swietach P, Spitzer KW & Vaughan Jones RD (2013). Intracellular Na^+ spatially controls Ca^{2+} signaling during acidosis in the ventricular myocyte. *Biophys J* **104** (Suppl. 1), 362a.

Swietach P & Vaughan-Jones RD (2005*a*). Relationship between intracellular pH and proton mobility in rat and guinea-pig ventricular myocytes. *J Physiol* **566**, 793–806.

Swietach P & Vaughan-Jones RD (2005*b*). Spatial regulation of intracellular pH in the ventricular myocyte. *Ann N Y Acad Sci* **1047**, 271–282.

Swietach P, Youm Y, Saegusa N, Leem C, Spitzer KW & Vaughan-Jones RD (2012). Role of cytoplasmic buffers in spatial H^+-Ca^{2+} interactions in ventricular myocytes. *Proc Physiol Soc* **27**, PC8.

Swietach P, Zaniboni M, Stewart AK, Rossini A, Spitzer KW & Vaughan-Jones RD (2003). Modelling intracellular H^+ ion diffusion. *Prog Biophys Mol Biol* **83**, 69–100.

Vaughan-Jones RD, Peercy BE, Keener JP & Spitzer KW (2002). Intrinsic H^+ ion mobility in the rabbit ventricular myocyte. *J Physiol* **541**, 139–158.

Vaughan-Jones RD, Spitzer KW & Swietach P (2009). Intracellular pH regulation in heart. *J Mol Cell Cardiol* **46**, 318–331.

Wei S, Guo A, Chen B, Kutschke W, Xie YP, Zimmerman K, Weiss RM, Anderson ME, Cheng H & Song LS (2010). T-tubule remodeling during transition from hypertrophy to heart failure. *Circ Res* **107**, 520–531.

Willoughby D & Schwiening CJ (2002). Electrically evoked dendritic pH transients in rat cerebellar Purkinje cells. *J Physiol* **544**, 487–499.

Yamamoto T, Swietach P, Rossini A, Loh SH, Vaughan-Jones RD & Spitzer KW (2005). Functional diversity of electrogenic Na^+-HCO_3^{--} cotransport in ventricular myocytes from rat, rabbit and guinea pig. *J Physiol* **562**, 455–475.

Yokoyama H, Gunasegaram S, Harding SE & Avkiran M (2000). Sarcolemmal Na^+/H^+ exchanger activity and expression in human ventricular myocardium. *J Am Coll Cardiol* **36**, 534–540.

Zaniboni M, Swietach P, Rossini A, Yamamoto T, Spitzer KW & Vaughan-Jones RD (2003). Intracellular proton mobility and buffering power in cardiac ventricular myocytes from rat, rabbit, and guinea pig. *Am J Physiol Heart Circ Physiol* **285**, H1236–H1246.

Author contributions

C.D.G. and R.D.V.-J. conceived and designed the experiments; C.D.G, Y.-L.M, P.S. and L.H. collected and analysed data; C.D.G and R.D.V.-J wrote the paper with input from P.S. All authors approved the final version of the manuscript.

Acknowledgements

We wish to thank J. Praetorius (Aarhus University, Denmark) for kindly providing antibodies for NBCe2 and NBCn1, Kenneth Spitzer and Gregory Lim who assisted with some of the early cell detubulation experiments, and Philip Cobden and Mala Rohling for expert technical assistance with cell isolation. This work was supported by the British Heart Foundation Programme Grant RG/08/016 to R.D.V.-J and by the Royal Society grant to P.S.

Supplemental Data

1-***Immunofluorescence NBCe2*** Immunofluorescence experiments with an antibody raised against NBCe2 N-terminus produced non-specific staining (scale bar: 25 μM). A 120 kDa band, consistent with NBCe2, was detected by western blot, but there were also several non-specific bands.

2- ***Dimensions of control and detubulated myocytes*** Dimensions of control and detubulated myocytes. Measurements of length (*l*) and width (*w*) were taken from transmission images, as illustrated. *xy* area was measured as the surface outlined (ImageJ), or calculated as the product of width by length, assuming rectangular shape. The product *wl* (estimated area) provides a good approximation of the measured area. Values obtained from 10 control and 26 detubulated cells, differences are not significant.

3- ***NHE1 distribution in quiescent and electrically-stimulated myocytes.*** Electrical stimulation (5 Hz for 5 min in Hepes buffer, *n*=8) produced no change in the distribution pattern of NHE1 in the membrane of cardiomyocytes ie. NHE1 remains excluded from t-tubules. Scale bar 40 μm.

NBCe2

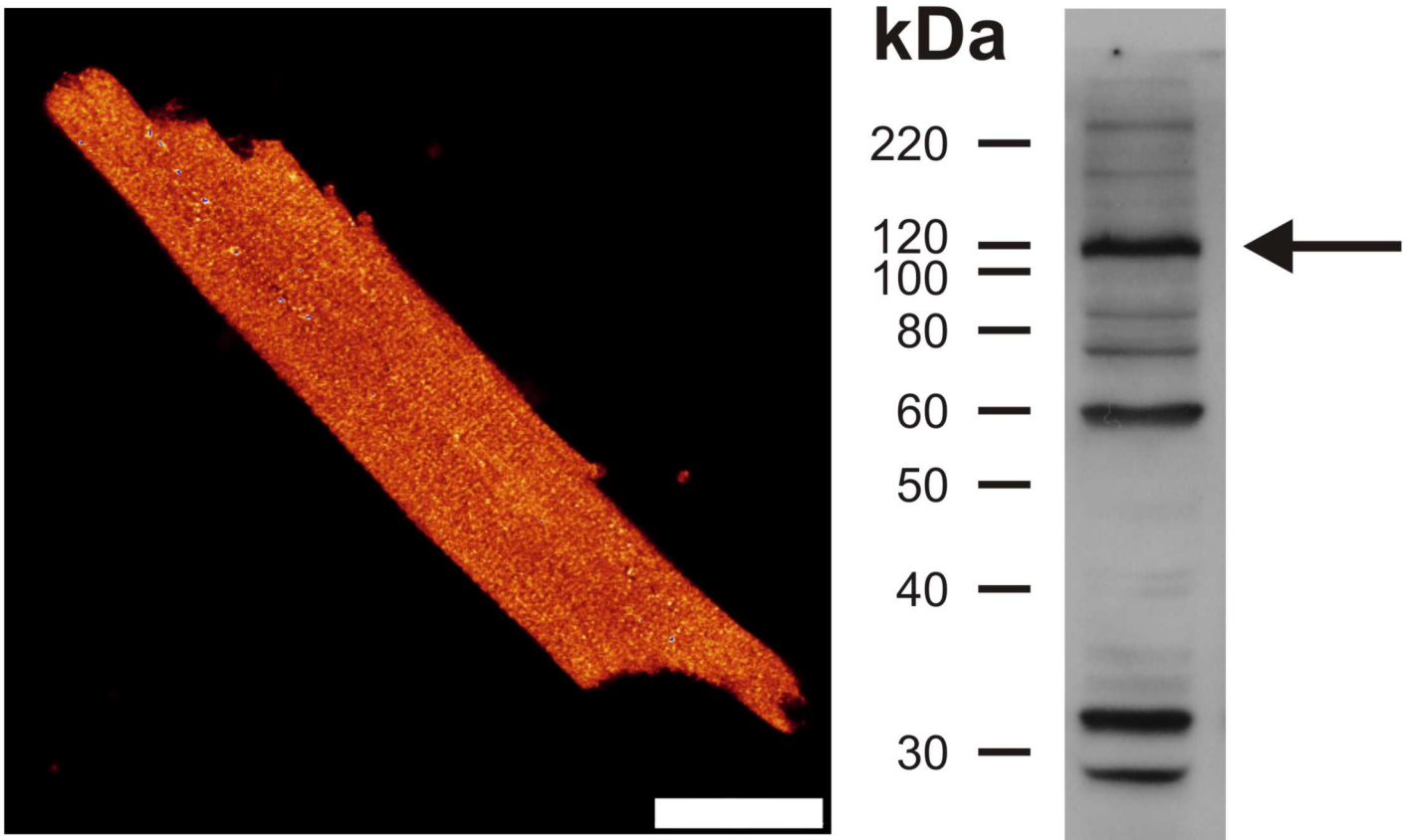

supplemental figure 1

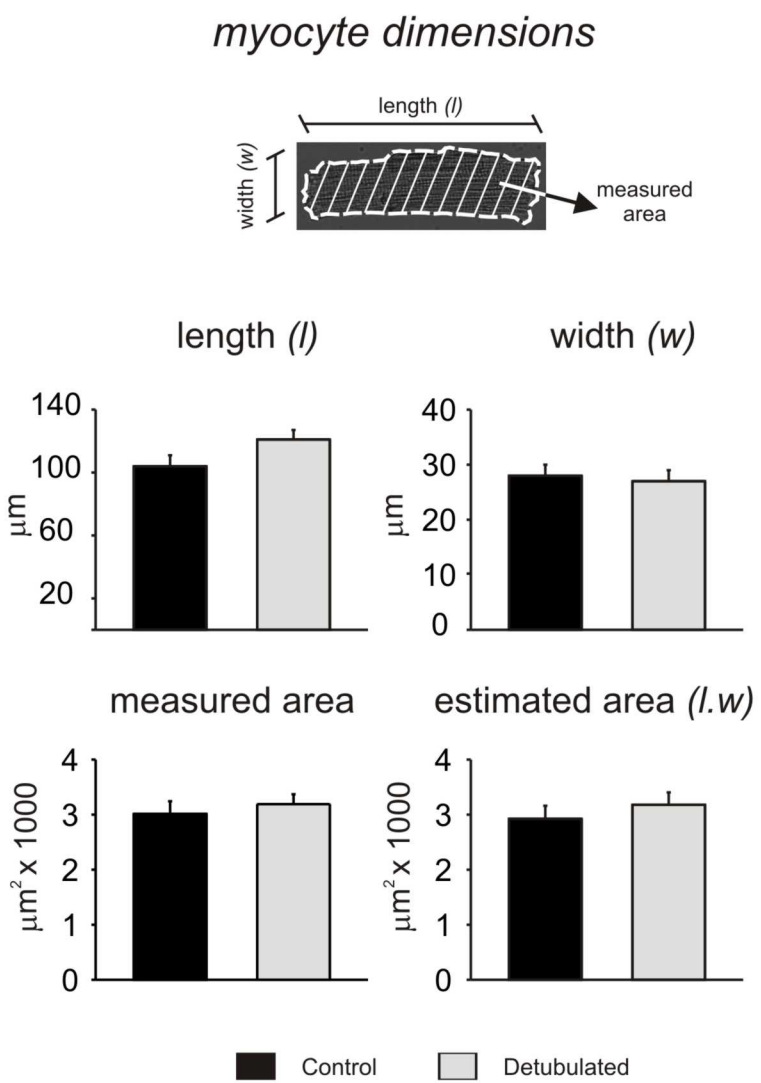

supplemental figure 2

supplemental figure 3